Munc18-1 redistributes in nerve terminals in an activity- and PKC-dependent manner

Tony Cijsouw, Jens P. Weber, Jurjen H. Broeke, Jantine A.C. Broek, Desiree Schut, Tim Kroon, Ingrid Saarloos, Matthijs Verhage, and Ruud F. Toonen

Department of Functional Genomics and Clinical Genetics, Center for Neurogenomics and Cognitive Research, Neuroscience Campus Amsterdam, VU University Amsterdam and VU Medical Center, 1081 HV Amsterdam, Netherlands

Munc18-1 is a soluble protein essential for synaptic transmission. To investigate the dynamics of endogenous Munc18-1 in neurons, we created a mouse model expressing fluorescently tagged Munc18-1 from the endogenous *munc18-1* locus. We show using fluorescence recovery after photobleaching in hippocampal neurons that the majority of Munc18-1 trafficked through axons and targeted to synapses via lateral diffusion together with syntaxin-1. Munc18-1 was strongly expressed at presynaptic terminals, with individual synapses showing a large variation in expression. Axon–synapse exchange rates of Munc18-1 were high: during stimulation, Munc18-1 rapidly dispersed from synapses and reclustered within minutes. Munc18-1 reclustering was independent of syntaxin-1, but required calcium influx and protein kinase C (PKC) activity. Importantly, a PKC-insensitive Munc18-1 mutant did not recluster. We show that synaptic Munc18-1 levels correlate with synaptic strength, and that synapses that recruit more Munc18-1 after stimulation have a larger releasable vesicle pool. Hence, PKC-dependent dynamic control of Munc18-1 levels enables individual synapses to tune their output during periods of activity.

Introduction

Synaptic vesicle fusion is executed by Sec1/Munc18 (SM) proteins and the multisubunit SNARE protein complex of synaptobrevin-2/VAMP2, syntaxin-1, and SNAP25 (Jahn and Scheller, 2006; Jahn and Fasshauer, 2012; Rizo and Südhof, 2012). The SM protein Munc18-1 is a soluble protein initially found as an interacting partner of syntaxin-1 (Hata et al., 1993; Garcia et al., 1994; Pevsner et al., 1994). Deletion of *munc18-1* completely arrests synaptic transmission (Verhage et al., 2000), whereas increased Munc18-1 levels result in a larger readily releasable vesicle pool (RRP) and increased synaptic efficacy (Toonen et al., 2006b). Mutations in *munc18-1* are found in patients with epilepsy and intellectual disability, and Munc18-1 dysregulation is implicated in Alzheimer's disease and schizophrenia (Jacobs et al., 2006; Saitsu et al., 2008; Hamdan et al., 2009; Milh et al., 2011; Vatta et al., 2012; Mastrangelo et al., 2013; Urigüen et al., 2013). Hence, Munc18-1 is required for normal brain function and its global expression levels scale with synaptic strength. However, the molecular mechanisms that control its synaptic levels are largely unknown.

Munc18-1 binds syntaxin-1 with high affinity, clamping syntaxin-1 in a conformation unable to bind other SNARE proteins (Dulubova et al., 1999; Misura et al., 2000). This interaction may stabilize both proteins and support their trafficking, as abrogated Munc18-1 expression results in aberrant targeting of syntaxin-1 in heterologous cells (Rowe et al., 2001; Medine et al., 2007; McEwen and Kaplan, 2008) and reduced expression levels of syntaxin-1 in neurons (Verhage et al., 2000; Voets et al., 2001; Zhou et al., 2013). In contrast, Munc18-1 levels are reduced in syntaxin-1 knockdown neurons (Zhou et al., 2013).

In developing neurons, syntaxin-1 is transported on vesicles via pathways dependent on the kinesin adaptor proteins syntabulin (Su et al., 2004) and FEZ1 (Chua et al., 2012). Munc18-1 is present in syntaxin–FEZ1–kinesin transport complexes (Chua et al., 2012). At this stage, the syntaxin-1/Munc18-1 dimer may

Correspondence to Matthijs Verhage: matthijs.verhage@cncr.vu.nl; or Ruud F. Toonen: ruud.toonen@cncr.vu.nl

Abbreviations used in this paper: AP, action potentials; BoNT/C, botulinum neurotoxin C; DIV, days in vitro; E, embryonic day; EPSC, excitatory postsynaptic current; ES, embryonic stem; FDR, false discovery rate; mVenus, membrane-targeted Venus protein; M-W, Mann-Whitney; RRP, readily releasable vesicle pool; Stx-YFP, syntaxin-1–enhanced YFP; WT, wild type.

The Rockefeller University Press $30.00
J. Cell Biol. Vol. 204 No. 5 759–775
www.jcb.org/cgi/doi/10.1083/jcb.201308026

function as a co-chaperone complex aiding transport and preventing premature breakdown of its constituents. However, in mature neurons syntaxin-1 is mainly transported via lateral diffusion along the plasma membrane (Mitchell and Ryan, 2004; Ribrault et al., 2011), and it is unknown whether at this stage Munc18-1 depends on syntaxin-1 for targeting to fusion sites.

To investigate the dynamics of endogenous Munc18-1 in neurons, we created mice expressing fluorescently tagged Munc18-1 from the endogenous *munc18-1* locus. We characterized Munc18-1 dynamics using FRAP in cultured hippocampal neurons at rest, during stimulation, and upon application of several active compounds. Munc18-1 trafficked through axons and to synapses with membrane-bound syntaxin-1. During stimulation, synaptic Munc18-1 rapidly dispersed from synapses and reclustered within minutes. This was independent of syntaxin-1 and synaptic vesicle fusion but required calcium influx and PKC activity. Hence, the presence of Munc18-1 in synapses is tightly regulated; during periods of activity Munc18-1 becomes more dynamic and reclusters at synapses in a phosphorylation-dependent way. Finally, we show that increased Munc18-1 recruitment correlates with increased strength of individual synapses.

Results

Munc18-1-Venus mice as reporters of endogenous Munc18-1

Munc18-1-Venus knock-in mice were generated with Venus cDNA, replacing the stop codon of exon 20 of *munc18-1* (Fig. 1 A) via homologous recombination in embryonic stem cells (Fig. 1 B). Wild-type (WT; +/+), Munc18-1-Venus heterozygous (+/m), and homozygous (m/m) genotypes were detected by PCR (Fig. 1 C). Total brain protein levels of Munc18-1-Venus in m/m mice were indistinguishable from Munc18-1 in +/+ littermates (Fig. 1, D and F), although Munc18-1-Venus levels were slightly reduced in +/m littermates (Figs. 1 D and S1), as was found in Munc 13-1-EYFP mice (Kalla et al., 2006). Munc18-1-Venus localization was comparable with Munc18-1 in WT brain with high expression in axonal fibers and mossy fiber terminals of the stratum lucidum in the hippocampus (Fig. 1 G).

The morphology and synapse number of hippocampal neurons from Munc18-1-Venus mice at 8 and 14 d in vitro (DIV) was similar to WT littermates (Fig. S1 and Fig. 2, A–D). Excitatory postsynaptic current (EPSC) amplitudes (Fig. 2 E), short-term plasticity (Fig. 2, H and K), spontaneous miniature EPSC frequency and amplitude (Fig. 2 H), and RRP size and recovery (Fig. 2, I–K) of Munc18-1-Venus autaptic hippocampal cultures were similar to WT. Hence, Munc18-1-Venus neurons can be used as functional reporters of Munc18-1 dynamics in living cells.

Munc18-1 transport in axons depends on syntaxin-1

In cultured neurons, membrane-bound syntaxin-1 diffuses laterally through the axon (Ribrault et al., 2011). Munc18-1 colocalizes with syntaxin-1 throughout the axon, and both proteins may be transported as a binary complex (Garcia et al., 1995; Ribrault et al., 2011). To test this, we imaged hippocampal neurons of Munc18-1-Venus mice at 14 DIV, when synaptic contacts are functional, and compared Munc18-1-Venus dynamics in axons with soluble GFP and membrane-bound syntaxin-1–enhanced YFP (Stx-YFP) using FRAP analysis. We bleached extended regions of single axons (Fig. 3, A–C) to discriminate fast recovery of freely diffusing GFP (Fig. 3 A) from relatively slow recovery typical for membrane-bound molecules like Stx-YFP (Fig. 3 B). Fluorescence recovery of Stx-YFP was gradual and bidirectional, but markedly different in speed and extent from soluble GFP (Fig. 3, A, B, and E). Bleaching of axonal Munc18-1-Venus resulted in similar bidirectional and gradual recovery (Fig. 3, C and D). Mean Munc18-1-Venus recovery was similar to Stx-YFP and significantly slower than GFP (Fig. 3 E). In developing neurons Munc18-1 is bound to transport vesicles (Chua et al., 2012). We observed Munc18-1-Venus puncta entering the bleached area in only 16% of Munc18-1-Venus axons (Fig. S2), with a minimal effect on total fluorescence recovery. Hence, the majority of Munc18-1 in axons of 14 DIV neurons, in contrast to developing neurons, does not bind transport vesicles. Munc18-1 also does not diffuse freely like GFP, but may move through axons by interacting with slowly diffusing proteins, like syntaxin-1.

To test this, we expressed botulinum neurotoxin C (BoNT/C) light chain in Munc18-1-Venus neurons 6–12 h before FRAP experiments. BoNT/C cleaves syntaxin-1 at the C terminus just above the transmembrane region (Blasi et al., 1993; Schiavo et al., 1995), detaching the remaining protein from the membrane and arresting synaptic vesicle fusion (de Wit et al., 2006). Fluorescence recovery of axonal Munc18-1-Venus in cells expressing BoNT/C was significantly faster than control cells (Fig. 3 F). BoNT/C expression does not affect electrical properties of neurons or neuronal morphology at the ultrastructural level (de Wit et al., 2006), making it unlikely that indirect effects of syntaxin-1 cleavage contributed to the observed Munc18-1 transport phenotype. Together, these results show that the majority of Munc18-1 does not diffuse freely but binds to syntaxin-1 for transport through the axon via lateral diffusion in the membrane.

Synaptic Munc18-1 dynamics are only partially syntaxin-1 dependent

Munc18-1 is expressed in synapses (Toonen and Verhage, 2007). Munc18-1-Venus fluorescence was high in presynaptic terminals identified by synapsin-mCherry (Fig. 4 A). The synapse-to-axon ratio of Munc18-1-Venus was significantly higher than a membrane-targeted Venus protein (mVenus, Fig. 4 B), which suggests that Munc18-1-Venus is retained at synapses. To test this, we used FRAP of Munc18-1-Venus, Stx-YFP, and GFP on single synapses (Fig. 4 C). A focused laser spot aimed at a single synapsin-mCherry punctum (Fig. 4 D, open arrowhead) bleached the synaptic region, and fluorescence recovery was followed over time (Fig. 4 D). The initial (at 10 and 30 s) recovery of synaptic Munc18-1-Venus was markedly slower than GFP and not significantly different from Stx-YFP, although the mobile fraction of Munc18-1-Venus was slightly smaller than Stx-YFP (Fig. 4 E). We then compared FRAP of Munc18-1-Venus in the presence or absence of BoNT/C. Mean fluorescence

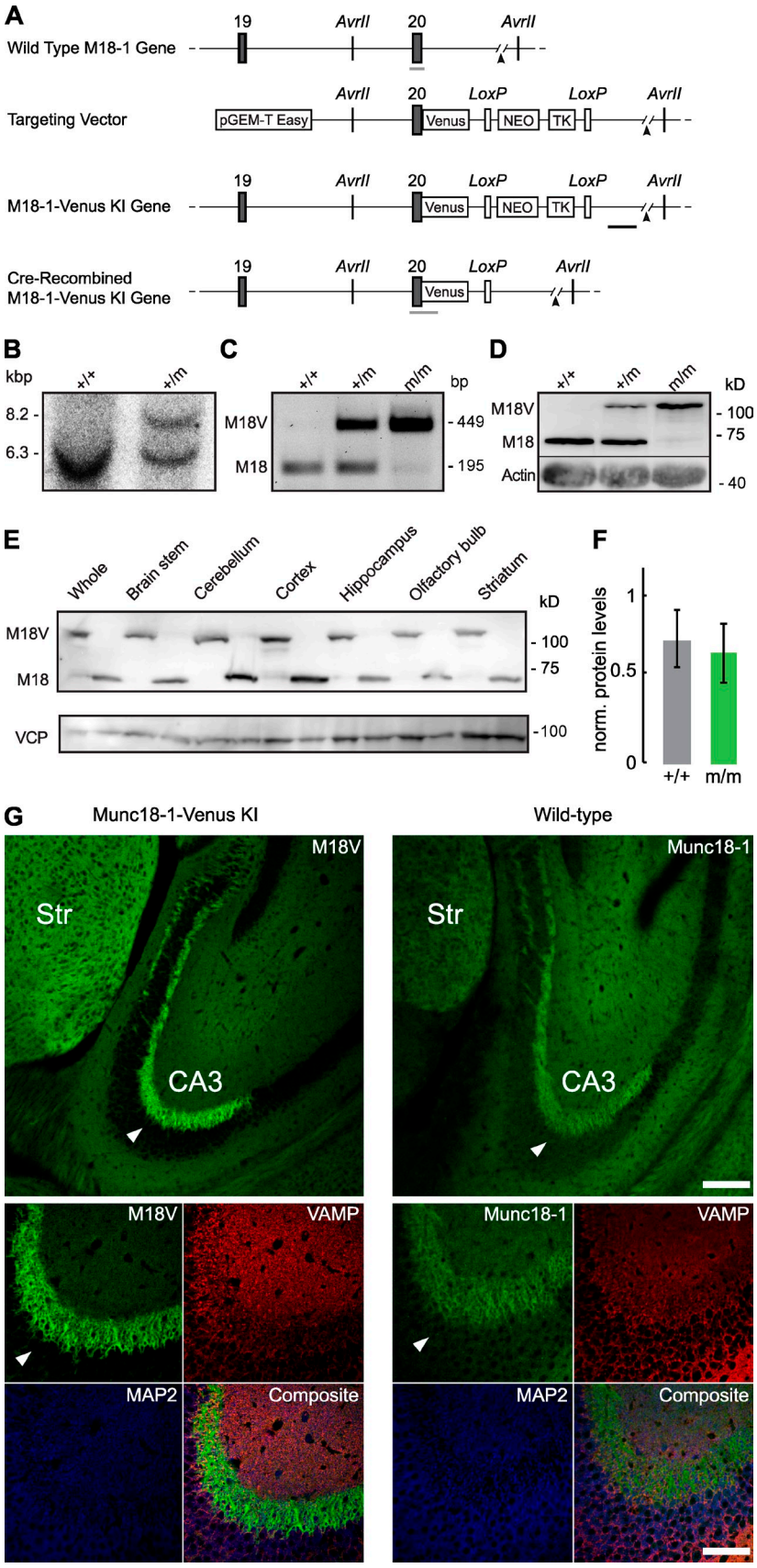

Figure 1. **Generation and confirmation of Munc18-1-Venus (M18V) mouse.** (A) Generation of M18V knockin gene. Diagrams indicate WT *munc18-1* gene, targeting vector, *M18V-neo-knock-in* gene, and Cre-recombined *M18V* gene. Exons are indicated by gray boxes and numbered. Black and gray horizontal bars indicate probes used for Southern blot analysis and PCR products used for genotyping, respectively. A 5-kbp section is not shown (arrowheads). *LoxP*, *loxP* sites; Venus, Venus cDNA; *AvrII*, restriction enzyme site; NEO, neomycin resistance gene; TK, thymidine kinase promoter; pGEM-T Easy, targeting vector. (B) Southern blot analysis of mouse tail DNA from heterozygous (+/m) and WT (+/+) mice. DNA was AvrII-digested. m, *M18V-neo-knock-in* gene (8.2 kbp); +, *munc18-1* gene (6.3 kbp). (C) Agarose gel of PCR products from +/+, +/m, and m/m mouse DNA. M18V, *munc18-1-Venus* gene PCR product, 449 bp; M18, *munc18-1* gene PCR product, 195 bp. (D) Western blot of brain lysate of +/+, +/m, and m/m mice stained for M18V. Actin was used as a loading control. The lines indicate that intervening lanes have been spliced out. (E) Western blot of brain region lysate of m/m and +/+ mice at E18 stained for M18V. Valosin-containing protein (VCP) was used as a loading control. (F) Quantification of M18V expression levels in +/+ and m/m brain lysate. Homogenates from +/+ and m/m brains were analyzed by SDS-PAGE (10 µg of protein per lane) and Western blotting with Munc18-1 antibodies. M18V protein levels were normalized to VCP protein levels for each mouse ($n = 6$). Error bars indicate mean ± SEM. (G) Hippocampal localization of M18V fluorescence in m/m (M18V homozygote) brain slice (left) and of antibody-stained Munc18-1 in WT (+/+) mice (right) compared with synaptic marker VAMP and dendritic marker MAP2. CA3, hippocampal CA region; Str, striatum; arrowheads, mossy fiber terminals of the stratum lucidum. Bars: (overview images) 100 µm; (enlarged panels) 25 µm.

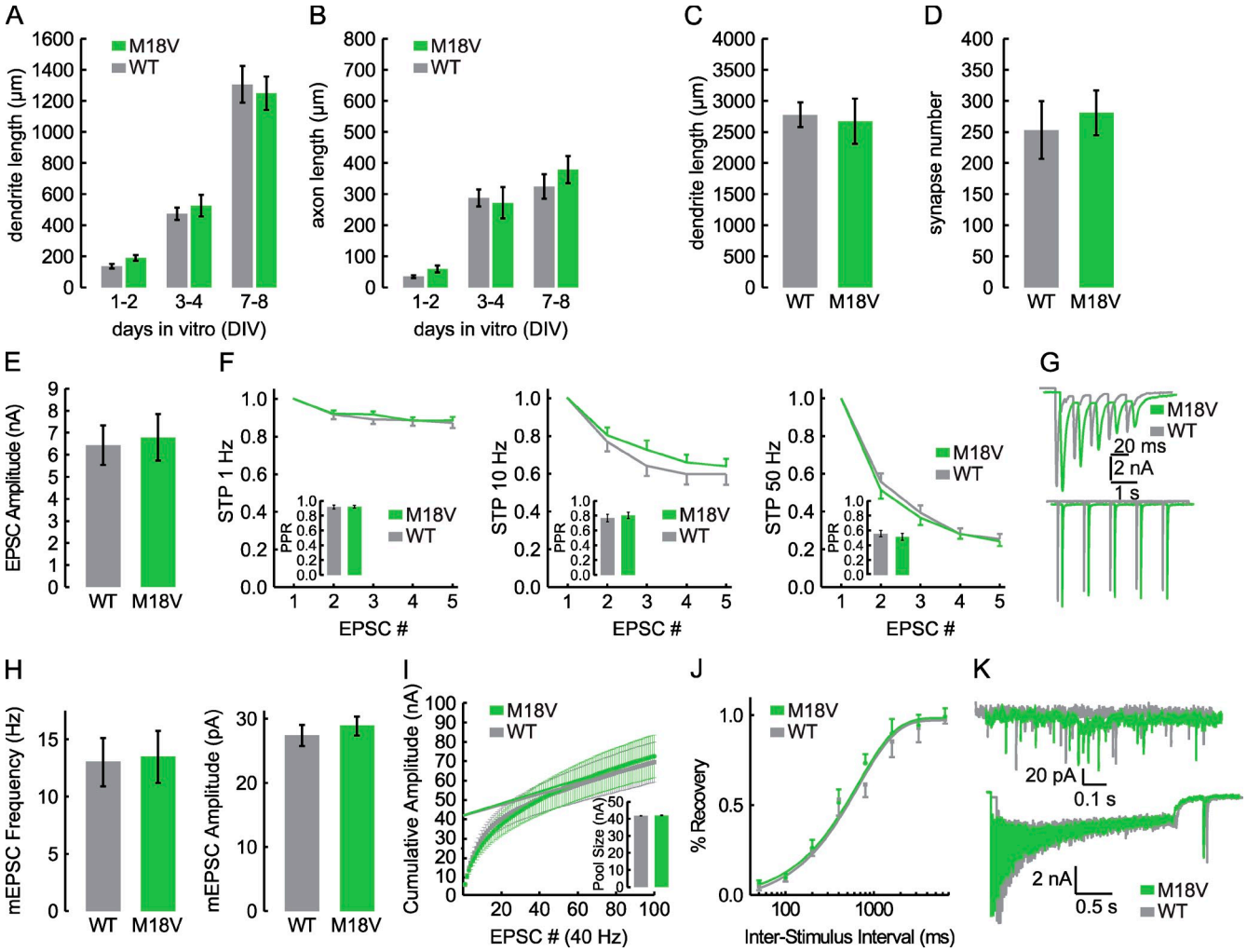

Figure 2. **Morphology and synaptic transmission of Munc18-1-Venus (M18V) hippocampal neurons is indistinguishable from WT neurons.** Shown are the characterization of neuron morphology (A–D) and electrophysiology (E–K) of WT (gray) and M18V (green) hippocampal autapse cultures. (A) Dendrite length was measured using MAP2 staining at 1–2 DIV, 3–4 DIV, and 7–8 DIV (M-W test: WT 1–2 DIV, n = 26 cells; M18V 1–2 DIV, n = 44 cells, P = 0.049; WT 3–4 DIV, n = 27 cells; M18V 3–4 DIV, 27 cells, P > 0.05; WT 7–8 DIV, n = 26 cells; M18V 7–8 DIV, 32 cells, P > 0.05). (B) Axon length measured using a cocktail of Smi-312 and Ankyrin G staining at 1–2 DIV, 3–4 DIV, and 7–8 DIV (M-W: WT 1–2 DIV, n = 26 cells; M18V 1–2 DIV, n = 44 cells, P > 0.05; WT 3–4 DIV, n = 27 cells; M18V 3–4 DIV, n = 27 cells, P > 0.05; WT 7–8 DIV, n = 26 cells; M18V 7–8 DIV, n = 32 cells, P > 0.05). (C) Dendrite length measured using MAP2 staining at DIV 14 (M-W test: WT, n = 32 cells; M18V, n = 27 cells, P > 0.05). (D) Synapse number per cell measured using synapsin staining at 14 DIV (unpaired t test: WT, n = 13 cells; M18V, n = 13 cells, P > 0.05). (E) Single evoked EPSC amplitudes (WT, 6.4 ± 0.9 nA, n = 22; M18V, 6.8 ± 1.0 nA, n = 24; M-W test, P > 0.05). (F) Normalized short-term plasticity (STP) curves with 5 EPSCs in 1 Hz (left), 10 Hz (middle), and 50 Hz (right) interstimulus intervals (ISI). (insets) Paired pulse ratios (PPRs; WT 1 Hz, 0.9180 ± 0.025, n = 14; M18V 1 Hz, 0.921 ± 0.017, n = 18; WT 10 Hz, 0.769 ± 0.049, n = 12; M18V 10 Hz 0.804 ± 0.041, n = 19; WT 50 Hz, 0.557 ± 0.044, n = 15; M18V 50 Hz, 0.514 ± 0.046, n = 19; M-W test, P > 0.05 for all). (G) Example traces for STP experiments at 50 Hz (top) and 1 Hz (bottom). (H) Frequency (left) and amplitude (right) of spontaneous miniature events (mEPSC; WT frequency, 13.1 ± 2.1 Hz, n = 19; M18V frequency, 13.5 ± 2.2 Hz, n = 20; WT amplitude, 27.4 ± 1.6 pA; M18V amplitude, 28.9 ± 1.4 pA; M-W test, P > 0.05). (I) Cumulative EPSC amplitudes in a 100 AP, 40 Hz train with readily releasable pool size estimation via steady-state back extrapolation (inset: pool size in WT, 41.9 ± 0.1 nA, n = 13; M18V, 42.1 ± 0.2 nA, n = 14; M-W test, P > 0.05). (J) RRP recovery after train depletion (using 100 AP at 40 Hz) and a test pulse with varying ISIs (Recovery tau: WT, 665 ms, n = 20; M18V, 659 ms, n = 15; M-W test, P > 0.05). (K) Example traces for spontaneous miniature EPSCs (top) and 100 AP, 40 Hz stimulus train with a recovery test pulse (ISI 400 ms; bottom). Error bars indicate mean ± SEM.

recovery of synaptic Munc18-1-Venus in BoNT/C-expressing cells was significantly larger than in control cells (Fig. 4 F) and resulted in an increased mobile fraction of Munc18-1-Venus (Fig. 4 G). Hence, deletion of syntaxin-1 increases the dynamics of synaptic Munc18-1-Venus, which indicates that synaptic retention of Munc18-1 is largely dependent on syntaxin-1. A small immobile Munc18-1-Venus pool remained upon BoNT/C treatment (Fig. 4 G), which suggests that this pool is retained by interactions with other synaptic proteins.

Synaptic Munc18-1 dynamics and levels change upon neuronal activity

Next, we tested whether Munc18-1 dynamics are modulated by activity by stimulating Munc18-1-Venus neurons while bleaching synaptic fluorescence during stimulation. Initial Munc18-1-Venus fluorescence recovery (after 10 and 30 s) in synapses stimulated with 600 action potentials (AP) at 20 Hz was indistinguishable from control synapses (Fig. 5 A). However, the mobile fraction (measured at 160 s) was significantly larger in

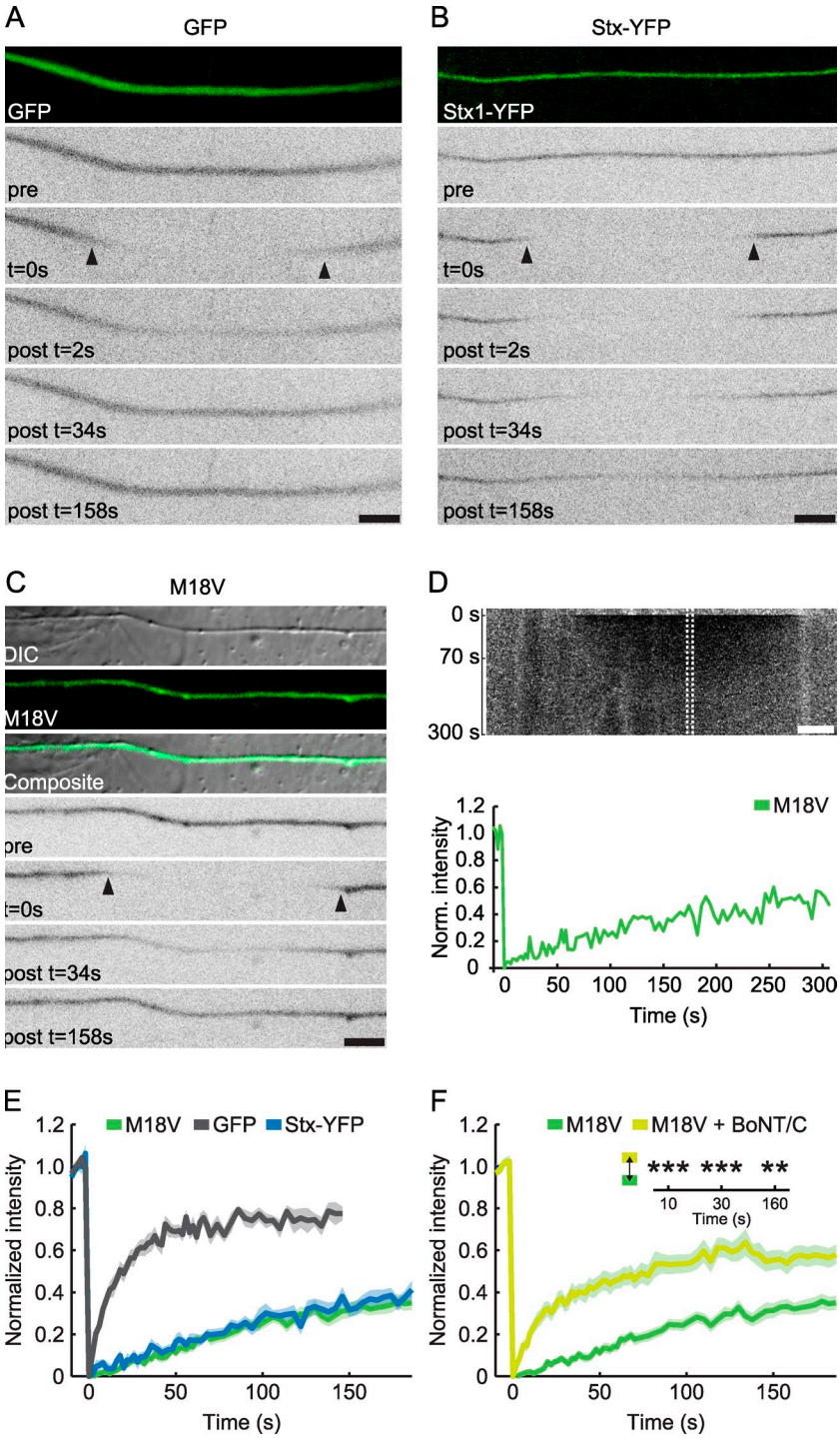

Figure 3. **Munc18-1-Venus dynamics in axons depend on syntaxin-1.** (A) Distal axon of WT neuron expressing GFP (green) used in FRAP experiments. Inverted greyscale images show time points before (pre) and immediately after photobleaching (t = 0 s), and during fluorescence recovery (post t = 2 s, post t = 34 s, and post t = 158 s). Arrowheads indicate the region of photobleaching. (B) Fluorescence image (green) and inverted greyscale images (same time points as in A) showing FRAP of a distal axon of WT neuron expressing syntaxin-1-EYFP (Stx-YFP). Note the difference in speed and the extent of recovery between soluble GFP and membrane-bound Stx-YFP. (C) Distal axon from a Munc18-1-Venus (M18V) neuron shown in differential interference contrast (greyscale), a fluorescence image (green), and a combined image (composite). Inverted greyscale images show time points before (pre) and immediately after bleaching (t = 0 s), and during fluorescence recovery (post t = 34 s and post t = 158 s). (D) Kymograph (top) and FRAP analysis (bottom) of the axon in C. The kymograph shows fluorescence recovery from both sides of the unbleached area. Fluorescence intensity was measured in the middle of the bleached area (broken lines) and normalized to prebleach and t = 0 s (see Materials and methods). (E) FRAP analysis of axonal M18V, Stx-YFP, and GFP. There were no statistically significant differences between M18V and Stx-YFP at t = 10 s, 30 s, and 160 s (M-W test with FDR [6] corrections: M18V, *n* = 7 cells, *n* = 15 axons, bleach length = 23.7 ± 1.3 µm; Stx-YFP, *n* = 16 field of views, *n* = 16 axons, bleach length = 25.2 ± 1.0 µm; GFP, *n* = 9 field of views, *n* = 9 axons, bleach length = 40.4 ± 2.9 µm). (F) FRAP analysis of axonal M18V (see E) and M18V + BoNT/C. (inset) Statistical significance (M-W test with FDR [6] corrections: ***, P < 0.001; **, P < 0.01; M18V + BoNT/C, *n* = 7 cells, *n* = 19 axons, bleach length = 25.7 ± 1.1 µm). Bars, 5 µm.

stimulated neurons (Fig. 5, A and B). We also probed Stx-YFP mobility using FRAP and found, in line with Ribrault et al. (2011), that initial recovery of Stx-YFP fluorescence was not affected by stimulation (Fig. 5 C). However, the mobile fraction (measured at 160 s) was increased (Fig. 5, C and D), similar to Munc18-1-Venus (Fig. 5, A and B). Thus, strong stimulation increases synaptic Munc18-1 and syntaxin-1 dynamics in hippocampal neurons.

Stimulation causes dispersion of several soluble synaptic proteins (Chi et al., 2001; Sankaranarayanan et al., 2003; Star et al., 2005; Denker et al., 2011), vesicle SNAREs (Li and Murthy, 2001; Fernández-Alfonso et al., 2006), and target SNAREs (Degtyar et al., 2013). To test whether Munc18-1 disperses from the synapse during stimulation, we measured intensity changes upon stimulation in Munc18-1-Venus neurons. Munc18-1-Venus was enriched in synapses identified by synapsin-mCherry before stimulation (Fig. 6 A). During stimulation, fluorescence of Munc18-1-Venus and synapsin-mCherry at synapses decreased (Fig. 6 A): Munc18-1-Venus fluorescence dispersed from the start of stimulation (Fig. 6 B), similar to

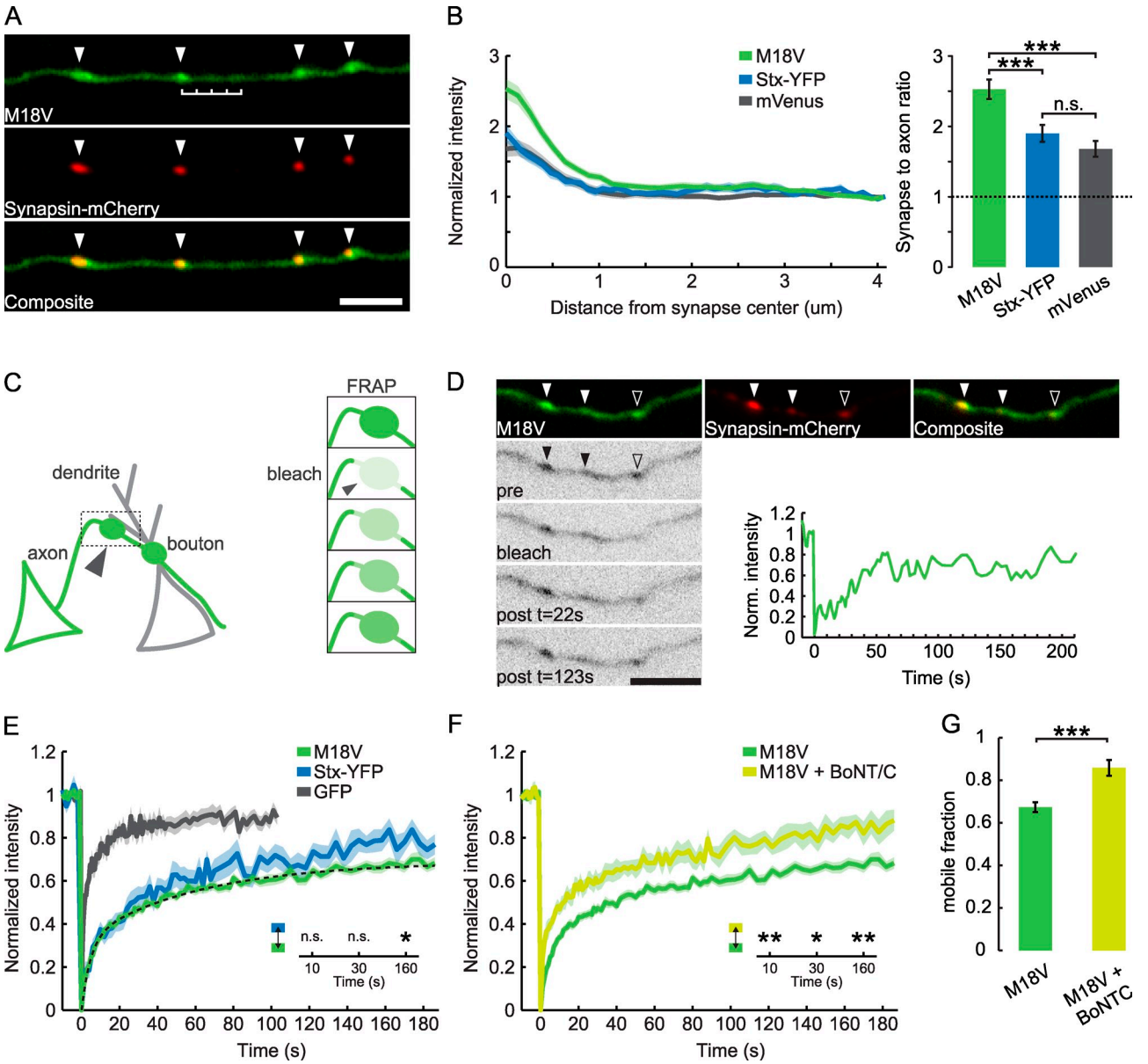

Figure 4. **Syntaxin-1 binding is the major determinant of an immobile Munc18-1 pool at synapses.** (A) Munc18-1-Venus (M18V) axon expressing synapsin-mCherry. Overlay of M18V and synapsin-mCherry fluorescence (Composite) shows Munc18-1-Venus expression at presynaptic sites. Bar, 4 µm. (B) Normalized fluorescence intensities of Stx-YFP and mVenus in WT neurons and M18V measured from the center of synapsin-mCherry positive puncta up to 4 µm into the axon (left; see scale bar in A). Intensity was normalized to axon intensity at 4 µm. Right, synapse (0 µm)-to-axon ratio (4 µm) of M18V, Stx-YFP, and mVenus (K-W test: ***, $P < 0.001$; n.s., $P > 0.05$; M18V, $n = 10$ field of views, $n = 72$ synapses; Stx-YFP, $n = 15$ field of views, $n = 58$ synapses; mVenus, $n = 12$ field of views, $n = 52$ synapses). (C) Diagram illustrating FRAP experiments shown in D–G. M18V neurons (green) expressing synapsin-mCherry as a synapse marker (not depicted) were cultured together with WT neurons (gray) in a 1:50 ratio. Fluorescence in synapses was photobleached (arrowheads and box) at t = 0 s, and fluorescence recovery was followed over time (FRAP, right). (D) M18V axon with three synapses (arrowheads) identified by synapsin-mCherry. Inverted greyscale images show time points before (pre), immediately after photobleaching (bleach, open arrowheads), and during fluorescence recovery (post t = 22 s and post t = 123 s). Bottom right, normalized intensity of bleached synapse over time. Bar, 5 µm. (E) FRAP analysis of synaptic M18V, GFP, and Stx-YFP. (inset) Statistical significance (M-W test with FDR [6] corrections: n.s., $P > 0.05$; *, $P < 0.05$; M18V, $n = 14$ field of views, $n = 37$ synapses; Stx-YFP, $n = 9$ field of views, $n = 23$ synapses; GFP, $n = 9$ field of views, $n = 28$ synapses). The broken line indicates a biexponential fit of M18V recovery with a fast mobile fraction of 0.32 and a tau of 4.6 s, and a slow mobile fraction of 0.36 and a tau of 59.8 s. (F) FRAP analysis of synaptic M18V (see E) and M18V + BoNT/C. (inset) Statistical significance (M-W test with FDR [6] corrections: **, $P < 0.01$; *, $P < 0.05$; M18V + BoNT/C, $n = 6$ cells, $n = 16$ synapses). (G) Mobile fraction of synaptic M18V compared with M18V + BoNT/C calculated from F at t = 180 s (M-W test: ***, $P < 0.001$). Error bars indicate mean ± SEM.

synapsin-mCherry (Chi et al., 2001; Fig. 6 B, inset). The intensity changes represented Munc18-1-Venus movement and not changes in Venus fluorescence due to proton-induced quenching (Nagai et al., 2002), as the fluorescence decrease of an mVenus was ninefold ($P < 0.001$) lower than the decrease in Munc18-1-Venus fluorescence (Fig. 6 C). Stx-YFP also dispersed from synapses (Fig. 6 B), although significantly less than Munc18-1-Venus (Fig. 6 C). Dispersion of Munc18-1-Venus and synapsin-mCherry required calcium influx and was impaired by superfusion of P/Q-, L-, and N-type calcium channel blockers (Fig. S5). To

test whether Munc18-1 dispersion required active vesicle release and syntaxin-1, we expressed BoNT/C. This did not affect Munc18-1-Venus dispersion (Fig. 6, D and E). Thus, stimulation-induced calcium influx triggers the dispersion of a fraction of synaptic Munc18-1-Venus into the axon. This dispersion is largely independent of syntaxin-1 and does not require synaptic vesicle release.

Munc18-1 reclusters at synapses after synaptic activity

Synapsin-1a fully reclusters to synapses within 10 min after synaptic activity (Chi et al., 2001). To test whether Munc18-1-Venus also reclusters at synapses, we followed synaptic Munc18-1-Venus fluorescence after stimulation. We observed a large variation in synaptic Munc18-1-Venus intensity changes (Fig. 7, A and B) that did not correlate with initial Munc18-1-Venus levels (Fig. S4). However, the mean response of all synapses showed dispersion during the stimulus, leading to a net increase in Munc18-1-Venus levels at t = 160 s (Fig. 7 C). This reclustering was much faster than synapsin-mCherry and was not observed for mVenus (Fig. S3). We defined two sets of synapses, one with initial dispersion ($\Delta F/F0 < 0$ at t = 10 s) followed by a net increase of fluorescence ($\Delta F/F0 > 0$ at t = 160 s, called $\Delta+$) and one with initial dispersion ($\Delta F/F0 < 0$ at t = 10 s) followed by a net decrease of fluorescence ($\Delta F/F0 < 0$ at t = 160 s, called $\Delta-$). Nearly half of all synapses fell in the $\Delta+$ subset and over one-third in the $\Delta-$ subset (Fig. 7 C). Unlike the increase observed for Munc18-1-Venus, Stx-YFP mean fluorescence remained below initial levels after dispersion with <25% $\Delta+$ synapses (Fig. 7 D). Reclustering was also slower than Munc18-1-Venus (Fig. 7 D). This suggests that Munc18-1-Venus reclusters faster than syntaxin-1 (and synapsin-mCherry), and independently of syntaxin-1. Indeed, synaptic Munc18-1-Venus fluorescence increased faster upon BoNT/C expression (Fig. 7, E and F) and resulted in higher levels at t = 160 s than in control neurons. Also, the percentage of $\Delta+$ synapses was higher upon BoNT/C (Fig. 7 E). Hence, reclustering of synaptic Munc18-1 does not require syntaxin-1, and is even enhanced in the absence of syntaxin-1. Munc18-1 reclustering was absent in neurons incubated with calcium channel blockers (Fig. 7, G and H; and Fig. S5, A–C). Hence, calcium influx as a result of synaptic activity increases Munc18-1 mobility and redistributes synaptic Munc18-1 levels such that on average synapses contain more Munc18-1 after a strong stimulus.

PKC-dependent phosphorylation of Munc18-1 is necessary for synaptic Munc18-1 reclustering

PKC-dependent phosphorylation of Munc18-1 is essential for DAG-induced potentiation of synaptic transmission (Wierda et al., 2007) and vesicle pool replenishment in chromaffin cells (Nili et al., 2006). To test if PKC activity modulates synaptic Munc18-1 dynamics, we applied the DAG analogue PMA to Munc18-1-Venus neurons. This did not significantly affect synaptic Munc18-1 levels (Fig. 8, A and B). PMA application during electrical stimulation did not further increase

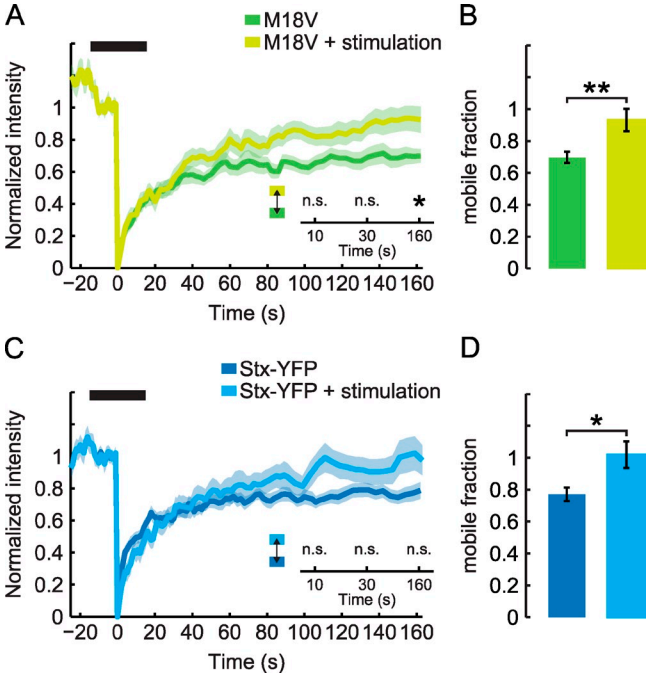

Figure 5. **Activity increases Munc18-1 and Syntaxin-1 mobility at synapses.** (A) FRAP analysis of Munc18-1-Venus (M18V) in control synapses and synapses stimulated with 600 AP at 20 Hz starting at t = −15 s (black bar). (inset) Statistical significance (M-W test with FDR [3] corrections: n.s., P > 0.05; *, P < 0.05; M18V, *n* = 8 field of views, *n* = 19 synapses; M18V + stimulation, *n* = 8 field of views, *n* = 16 synapses). (B) Mobile fraction of synaptic M18V, control compared with stimulation calculated from A at t = 160 s (M-W test: **, P < 0.01). (C) FRAP analysis of Stx-YFP in control synapses and synapses stimulated with 600 AP at 20 Hz starting at t = −15 s (black bar). (inset) Statistical significance (M-W test with FDR [3] corrections: n.s., P > 0.05; Stx-YFP, *n* = 6 field of views, *n* = 16 synapses; Stx-YFP + stimulation, *n* = 6 field of views, *n* = 13 synapses). (D) Mobile fraction of synaptic Stx-YFP control compared with stimulation calculated from C at t = 160 s (M-W test: *, P < 0.05). Error bars indicate mean ± SEM.

Munc18-1 recruitment after stimulation (Fig. 8, C and D) or its dynamics (Fig. S5). Hence, PMA application does not have an additive effect when PKC activity is triggered by calcium influx. However, application of the specific PKC inhibitor Ro 31-8220 (Davis et al., 1989) resulted in significantly less dispersion during stimulation and an almost complete block of Munc18-1-Venus reclustering after stimulation (Fig. 8, E and F). Ro 31-8220 application significantly reduced the number of synapses and mean recruitment in the $\Delta+$ subset (Fig. S5). Hence, PKC activity is required for reclustering of Munc18-1 after strong stimulation. Finally, to test whether PKC-dependent phosphorylation of Munc18-1 itself is required for its reclustering, we expressed a fully functional but PKC-insensitive mutant (PKC_i) of Munc18-1-EGFP (Wierda et al., 2007) in *munc18-1* null mutant neurons and compared its dynamics with WT Munc18-1-EGFP on the same null mutant background. In contrast to WT Munc18-1-EGFP, which behaved like Munc18-1-Venus, the PKC-insensitive mutant did not show reclustering after electrical stimulation (Fig. 8, G and H; and Fig. S5). This shows that activity-dependent PKC phosphorylation of Munc18-1 is essential to recruit Munc18-1 to synapses after neuronal stimulation.

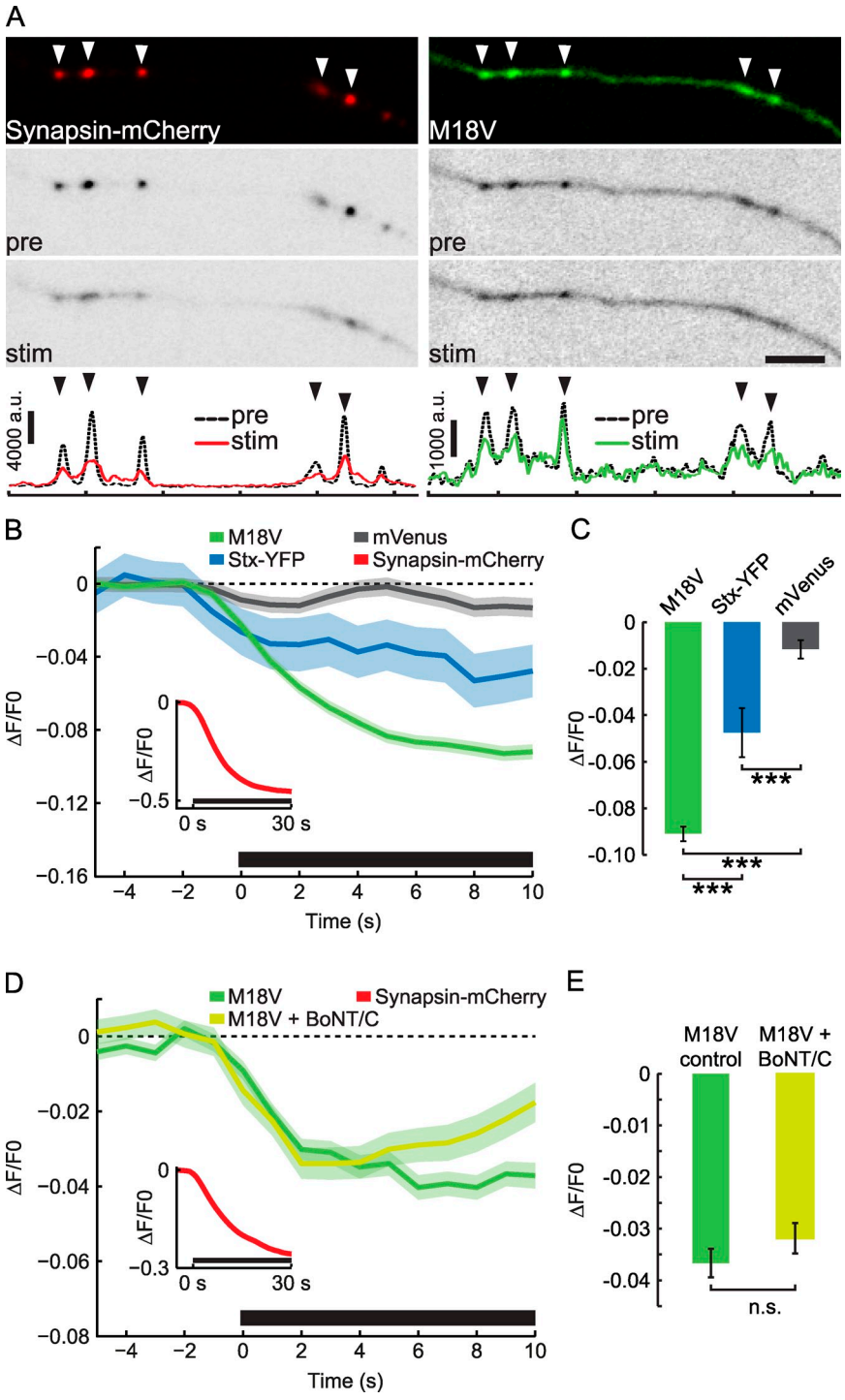

Figure 6. **Synaptic Munc18-1-Venus acutely disperses upon stimulation.** (A) Fluorescence and greyscale images of a Munc18-1-Venus (M18V) axon (right) expressing synapsin-mCherry (left). Greyscale images show the same axon before (pre) and during stimulation (stim) with 600 AP at 20 Hz. A linescan (bottom) along the axon compares fluorescence intensity in synapses marked with arrowheads of synapsin-mCherry before (pre, black broken line) with during (stim, red solid line) stimulation and intensity of M18V before (pre, black dashed line) with during (stim, green solid line) stimulation. Bar, 5 µm. (B) Relative intensity changes (ΔF/F0) of M18V, Stx-YFP, mVenus, and synapsin-mCherry (inset) at synapses during stimulation starting at t = 0 s (20 Hz, black bar). M18V and synapsin-mCherry, *n* = 38 field of views, *n* = 929 synapses; Stx-YFP, *n* = 17 field of views, *n* = 202 synapses; mVenus, *n* = 20 field of views, *n* = 305 synapses. (C) Relative intensity changes at t = 10 s of M18V, Stx-YFP, and mVenus calculated from B (K-W test: ***, P < 0.001). (D) Relative intensity changes (ΔF/F0) of M18V, M18V + BoNT/C, and synapsin-mCherry (inset) in synapses during stimulation starting at t = 0 s (20 Hz, black bar). M18V and synapsin-mCherry, *n* = 15 cells, *n* = 533 synapses; M18V + BoNT/C, *n* = 8 cells, *n* = 290 synapses. (E) Relative intensity changes of M18V and M18V + BoNT/C at t = 4 s calculated from D (M-W test: n.s., P > 0.05). Error bars indicate mean ± SEM. The horizontal broken line indicates no change.

Munc18-1 levels correlate with synaptic strength

Munc18-1 expression levels in neurons control synaptic strength by modulating the number of release-ready vesicles (Toonen et al., 2006b). To determine whether activity-dependent modulation of synaptic Munc18-1 levels affects presynaptic strength on a synapse level we probed vesicle release using FM4-64 uptake during 30 AP at 1 Hz, before and after high-frequency stimulation (Fig. 9 A). Individual synapses in naive neurons showed a large variation in Munc18-1-Venus levels and FM4-64 levels (Fig. 9 B). Interestingly, and in line with our previous results in Munc18-1–overexpressing neurons (Toonen et al., 2006b), synaptic Munc18-1-Venus levels showed a significant correlation with FM4-64 loading (Spearman's correlation $r_s = 0.27$, P < 0.001; Fig. 9 C), but not with synapse size (Fig. S4). Next, we tested whether a change in synaptic Munc18-1-Venus levels after high-frequency stimulation correlated with concomitant modulation in synaptic strength. We compared the change in FM4-64 uptake before and after 600 AP high-frequency stimulation between synapses with a

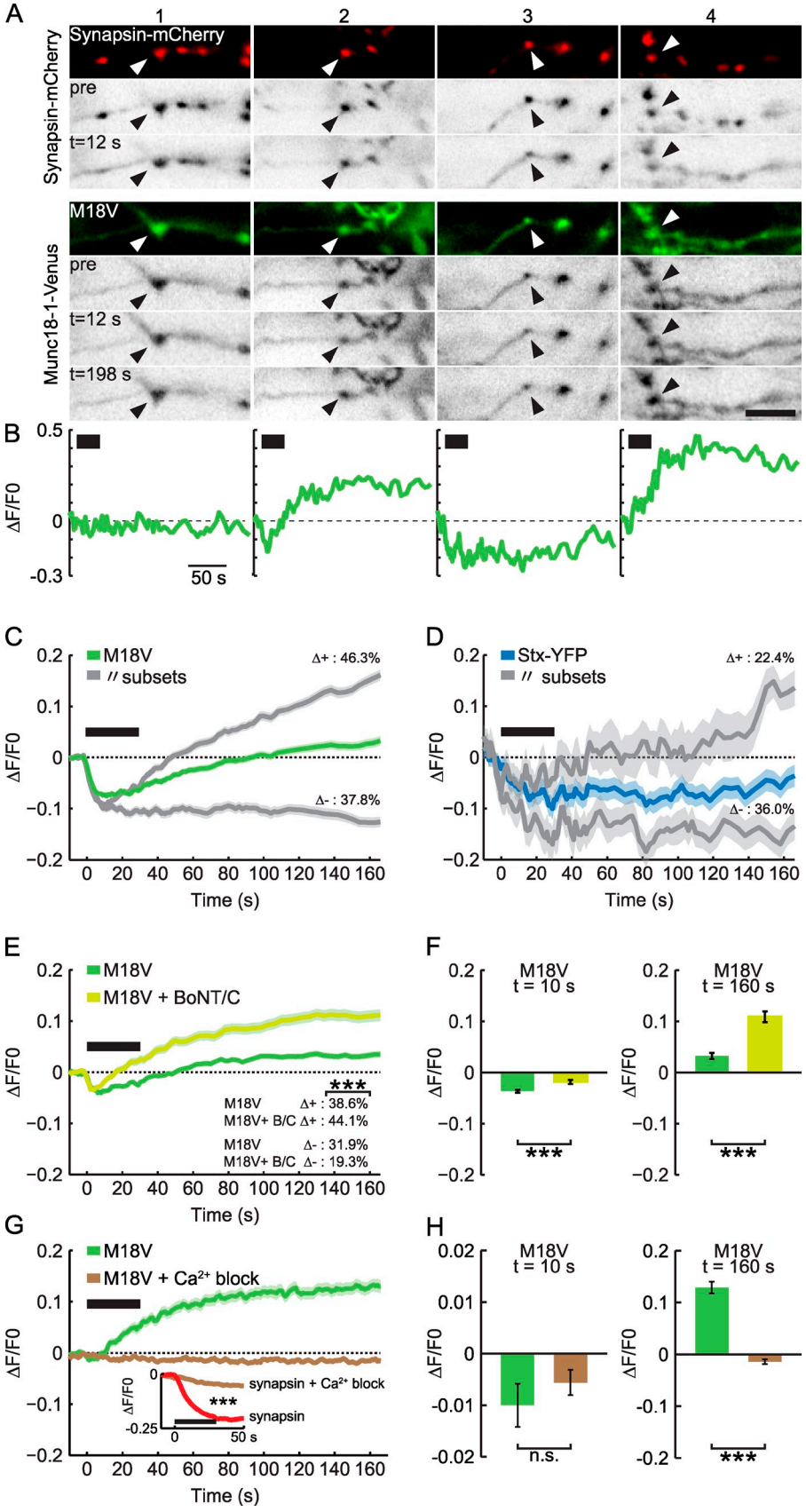

Figure 7. **Synaptic activity increases Munc18-1-Venus mobility and recruits Munc18-1 to synapses independent of syntaxin-1.** (A) Fluorescence and greyscale images of Munc18-1-Venus (M18V) axons expressing synapsin-mCherry. Greyscale images show the same axon before (pre), during (t = 12 s), and after stimulation (t = 198 s, M18V only) with 600 AP at 20 Hz (start t = 0 s). Bar, 5 µm. (B) Relative M18V intensity changes (ΔF/F0) in synapses marked by arrowheads in A. Black bars indicate the period of stimulation. Some synapses, after initial dispersion during stimulation, increase fluorescence above initial levels (broken line), whereas others remain low after initial dispersion or do not change during measurement. (C) Relative M18V intensity changes of all synapses (green line, *n* = 23 field of views, *n* = 510 synapses) compared with subsets (gray lines) of synapses with net positive change (Δ+, 46.3% of all synapses) and synapses with net negative change (Δ−, 37.8%) at t = 160 s. (D) Relative Stx-YFP intensity changes of all synapses (blue line, *n* = 10 field of views, *n* = 125 synapses) and of subsets (gray line) of synapses with net positive change (Δ+, 22.4% of all synapses) or a net negative change (Δ−, 36.0%) at t = 160 s. (E) Relative M18V intensity changes of all synapses (green, *n* = 5 cells, *n* = 553 synapses) and M18V ± BoNT/C synapses (yellow, *n* = 5 cells, *n* = 290 synapses). (inset) Percentage of synapses with net positive change (−BoNT/C, 38.6%; +BoNT/C, 44.1%) and synapses with net negative change (−BoNT/C, 31.9%; +BoNT/C, 19.3%) at t =160 s (Pearson χ^2 test: ***, P < 0.001). (F) Relative M18V intensity change at t = 10 s (left) and t = 160 s (right) at control synapses (green) and synapses expressing BoNT/C (yellow) calculated from E (M-W test with FDR [2] corrections: ***, P < 0.001). (G) Relative M18V and synapsin-mCherry (inset) intensity changes of control synapses (green, *n* = 6 cells, *n* = 250 synapses) and synapses superfused with calcium channel blockers to prevent calcium influx (brown, *n* = 6 cells, *n* = 252 synapses). Synapsin-mCherry intensity at t = 30 s, control versus calcium channel blockers, M-W test: ***, P < 0.001). (H) Relative M18V intensity change at t = 10 s (left) and t = 160 s (right) at control synapses (green) and synapses superfused with calcium channel blockers (brown) calculated from G (M-W test with FDR [2] corrections: n.s., P > 0.05; ***, P < 0.001). Note that although average dispersion (t = 10 s) in control synapses is lower compared with E, Fig. S5 shows that dispersion in Δ+ and Δ− control synapses is significantly higher than in synapses with calcium channel blockers. The horizontal broken line indicates no change.

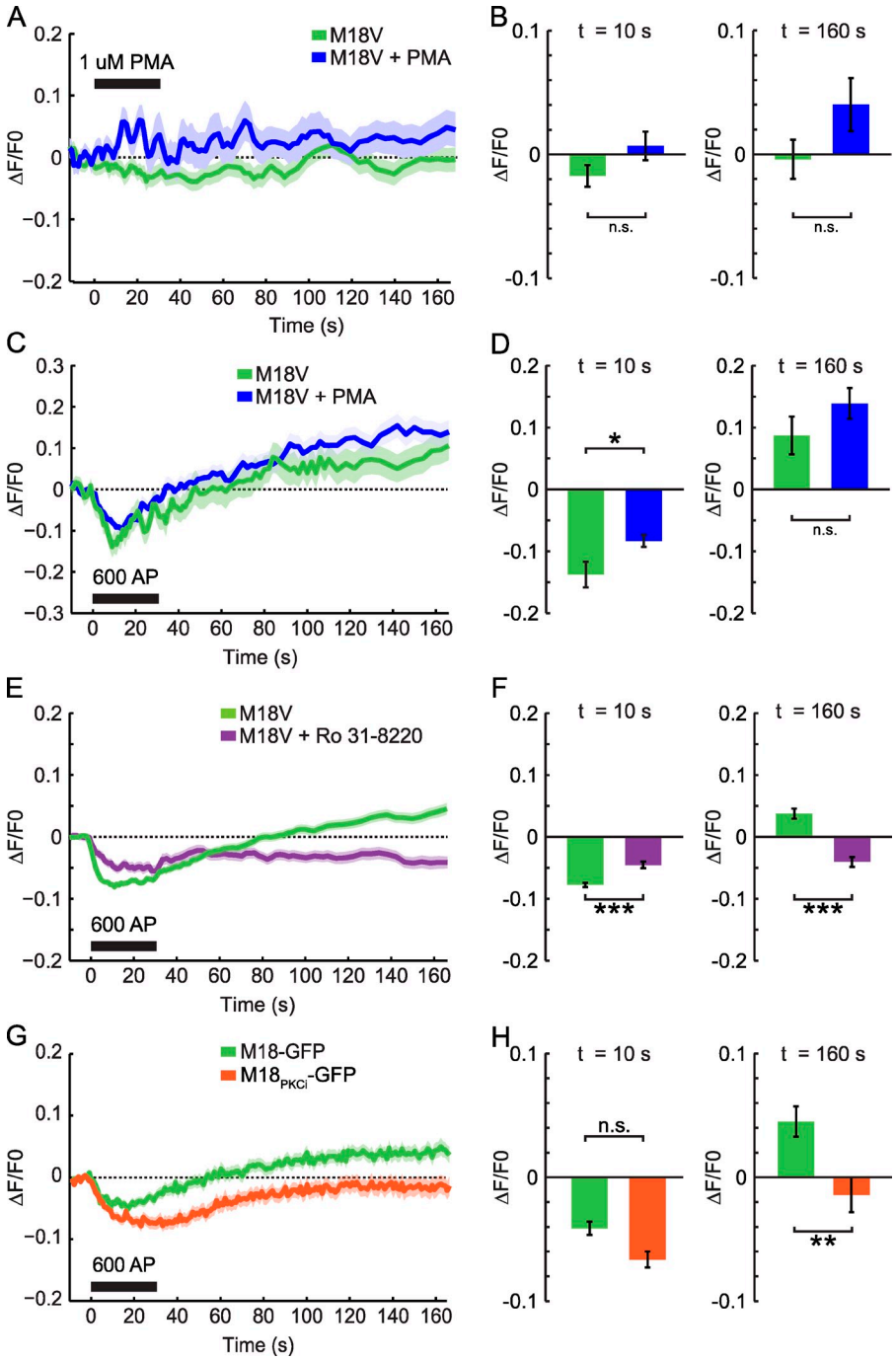

Figure 8. **PKC phosphorylation of Munc18-1 is necessary for synaptic recruitment.** (A) Relative Munc18-1-Venus (M18V) intensity changes (ΔF/F0) at control synapses (green, *n* = 9 field of views, *n* = 57 synapses) and synapses superfused with 1 µM PMA (blue, *n* = 6 field of views, *n* = 52 synapses) for 30 s at t = 0 s (black bar). (B) Relative M18V intensity change at t = 10 s (left) and t = 160 s (right) at control synapses and synapses with PMA calculated from A (M-W test with FDR [2] corrections: n.s., P > 0.05). (C) Relative M18V intensity changes after stimulation with 600 AP at 20 Hz starting at t = 0 s (black bar) at control synapses (green, *n* = 2 field of views, *n* = 43 synapses) and synapses with 1 µM PMA (blue, *n* = 7 field of views, *n* = 112 synapses) for >2 min (bath application). (D) Relative M18V intensity change at t = 10 s (left) and t = 160 s (right) at control synapses and synapses with PMA calculated from C (M-W test with FDR [2] corrections: n.s., P > 0.05; *, P < 0.05). (E) Relative M18V intensity changes after stimulation with 600 AP at 20 Hz starting at t = 0 s (black bar) at control synapses (green, *n* = 17 field of views, *n* = 465 synapses) and synapses with 1 µM Ro 31-8220 (purple, *n* = 11 field of views, *n* = 181 synapses). (F) Relative M18V intensity change at t = 10 s (left) and t = 160 s (right) at control synapses (green) and synapses with Ro 31-8220 (purple) calculated from E (M-W test with FDR [2] corrections: ***, P < 0.001). (G) Relative M18-GFP (green, *n* = 5 cells, *n* = 140 synapses) and $M18_{PKCi}$-GFP (orange, *n* = 3 cells, *n* = 84 synapses) intensity changes at synapses. (H) Relative M18-GFP and $M18_{PKCi}$-GFP intensity change at t = 10 s (left) and t = 160 s (right) at synapses calculated from G (M-W test with FDR [2] corrections: n.s., P > 0.05; **, P < 0.01). Error bars indicate mean ± SEM. The horizontal broken line indicates no change.

net positive reclustering of Munc18-1-Venus and synapses with a net negative reclustering. Synapses with positive reclustering had significantly more FM4-64 uptake compared with synapses having a net negative reclustering after high-frequency stimulation (20 Hz; Fig. 9 D). Synapses that were stimulated at low frequency (2 Hz; Fig. 9 D) did not show such a correlation. Together, these results show that synaptic Munc18-1-Venus levels scale with release efficiency and that changes in levels after high-frequency stimulation correlate with increased synaptic strength.

Discussion

Here, we investigated the distribution and dynamics of endogenous Munc18-1 in axons and synapses using Munc18-1-Venus knockin mice. In line with its essential role in exocytosis, we found that Munc18-1 is highly expressed in synapses. The majority of Munc18-1 traffics through axons via lateral diffusion together with syntaxin-1. Exchange rates of Munc18-1 at individual synapses are high compared with active zone components Bassoon and Munc13-1 (Kalla et al., 2006; Tsuriel et al., 2009).

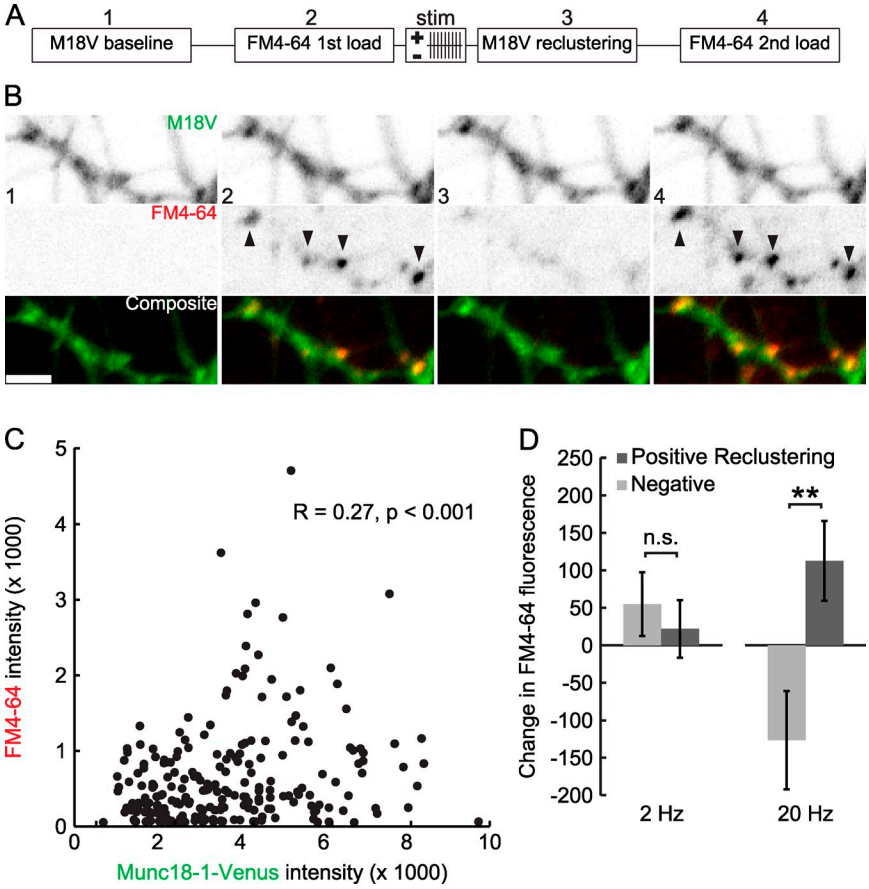

Figure 9. **Dynamic Munc18-1-Venus levels correlate with release of synaptic vesicles.** (A) Experimental design to probe synaptic release before and after stimulation that induces synaptic Munc18-1-Venus (M18V) dispersion and reclustering. (1) Baseline M18V fluorescence in synapses of naive M18V neurons. (2) First FM4-64 loading using 30 AP at 1 Hz in same synapses. Stim: 600 AP at 20 Hz (high frequency) or 2 Hz (low frequency, does not induce M18V dispersion). (3) FM4-64 unloading and M18V reclustering after 600 AP at 20 Hz. (4) Second FM4-64 loading using 30 AP at 1 Hz. Synapses were followed over time using synapsin-CFP (not depicted). (B) Greyscale and fluorescence images showing four stages of the experiment to probe synaptic release (see A) with FM4-64 loading (middle) in a M18V neuron (top). Composite (bottom) shows colocalization of M18V with FM4-64 puncta (arrowheads). Bar, 5 µm. (C) Initial M18V fluorescence (see A, 1) plotted against the first FM4-64 loading (see A, 2) of individual synapses (Spearman's correlation $r_s = 0.27$, $P < 0.001$; $n = 11$ field of views, $n = 232$ synapses). (D) Change in FM4-64 loading (between the first and second load) in synapses with a net positive and net negative reclustering of Munc18-1-Venus after 600 AP at 2 Hz or 20 Hz stimulation (*t* test: n.s., $P > 0.05$; **, $P = 0.006$; 2 Hz, $n = 4$ field of views, $n = 146$ synapses; 20 Hz, $n = 7$ field of views, $n = 195$ synapses). Error bars indicate mean ± SEM.

During periods of synaptic activity, Munc18-1 becomes even more dynamic, rapidly disperses, and subsequently reclusters at synapses. This requires calcium influx and PKC-dependent phosphorylation of Munc18-1, but is independent of syntaxin-1 interaction. Importantly, synaptic Munc18-1 levels scale with release efficiency, and higher Munc18-1 levels after stimulation increase synaptic strength.

Munc18-1 axonal transport in mature neurons is largely syntaxin-1 dependent

During neuronal development, Munc18-1/syntaxin-1 and syntaxin-1 are transported by FEZ1–KIF5C (Chua et al., 2012) and syntabulin–KIF5B (Su et al., 2004; Cai et al., 2007) transport complexes. Our FRAP experiments in axons (Fig. 3) showed identical recovery of Munc18-1-Venus and Stx-YFP and increased Munc18-1-Venus recovery after cleavage of syntaxin-1, which indicates that lateral diffusion via membrane-bound syntaxin-1 rather than active transport of organelles is the main mode of delivering Munc18-1 to release sites in mature neurons. This is in line with a study on syntaxin-1 dynamics in mature rat neurons (Ribrault et al., 2011), underscoring the notion that after initial membrane delivery via fusion of transport vesicles, Munc18-1–syntaxin-1 complexes diffuse through the axonal membrane. Only rarely were moving Munc18-1-Venus puncta observed, which suggests that vesicular transport of Munc18-1–syntaxin-1 complexes does continue in mature neurons but that diffusion dominates. Hence, during neuronal maturation, the mode of syntaxin/Munc18 transport switches from predominantly vesicular transport (Cai et al., 2007; Chua et al., 2012) to lateral diffusion.

Munc18-1 is highly dynamic at individual synapses

Munc18-1-Venus showed a strong synaptic preference (Fig. 4). Our FRAP measurements revealed that synaptic Munc18-1 is very mobile. Munc18-1-Venus exchange is best described with a fast ($\tau = 4.6$ s) and a slow component ($\tau = 60$ s), comparable to syntaxin-1 (Ribrault et al., 2011), whereas Bassoon (Tsuriel et al., 2009; Schröder et al., 2013), Munc13-1 (Kalla et al., 2006), liprin-α2 (Spangler et al., 2013), and synapsin-1 (Tsuriel et al., 2006) turnover at synapses is much slower, with exchange rates in the order of minutes to hours. Exchange rates of the total synaptic vesicle pool are even slower (Orenbuch et al., 2012b), although individual synaptic vesicle exchange between boutons is relatively fast (Darcy et al., 2006; Staras et al., 2010; Herzog et al., 2011). Synaptic activity increased the mobility of Munc18-1-Venus and Stx-YFP (Fig. 5), in line with increased mobility of synapsin (Chi et al., 2001; Tsuriel et al., 2006) and Rab3 (Star et al., 2005). In contrast, Munc13-1 and Bassoon mobility are not affected by acute stimulation (Kalla et al., 2006; Tsuriel et al., 2009). Hence, synapses exchange their components at different speeds. Proteins of the secretory machinery are more mobile than active zone scaffolding proteins and become even more dynamic during increased activity. The scaffolding proteins may therefore provide synapses with stability to maintain synapse integrity (Tsuriel et al., 2009),

whereas intersynaptic exchange of presynaptic molecules and vesicles provides plasticity during increased network activity.

At synapses, ∼40% of Munc18-1-Venus resided in an immobile fraction. Cleavage of syntaxin-1 resulted in a larger mobile Munc18-1-Venus fraction, but did not fully abolish the immobile fraction. This suggests that Munc18-1 also interacts with other binding partners at the synapse. Here, Munc18-1 may be released when syntaxin-1 interacts with other SNAREs, which lowers the binding affinity of Munc18-1 for syntaxin-1 (Xu et al., 2010). Strong interaction between Munc18-1 and syntaxin-1 in the axon may ensure proper delivery of Munc18-1 to synapses and protect syntaxin-1 from nonspecific interactions. A more dynamic interaction at the synapse provides plasticity to modulate SNARE complex formation and interactions of Munc18-1 with other proteins.

Synaptic activity acutely reorganizes synaptic Munc18-1 levels

Synaptic activity triggers synapsin dispersion from synapses (Chi et al., 2001; Fig. 6). In the same synapses, we observed significant Munc18-1-Venus dispersion during stimulation. Stx-YFP also dispersed, although to a smaller extent, which is in line with recent results (Degtyar et al., 2013). Dispersion of Munc18-1-Venus was not affected by BoNT/C expression (Fig. 6). Thus, calcium influx triggers dispersion irrespective of vesicle fusion, thereby increasing the concentration of soluble and dynamic Munc18-1.

Munc18-1 repopulated the synapse within 2 min after stimulation, much faster than synapsin (Chi et al., 2001; Orenbuch et al., 2012a) and Rab3a (Star et al., 2005), and reclustering already started during the stimulation train. On average, synapses contained more Munc18-1 after stimulation. Interestingly, post-stimulation changes in Munc18-1-Venus levels were highly variable: some synapses showed an ∼20% increase in fluorescence, whereas others showed an ∼10% net decrease (Fig. 7). Such distinct and acute changes in synaptic levels have not been reported before. As Munc18-1 expression levels correlate with synaptic strength and stamina (Toonen et al., 2006b), this provides a mechanism that helps individual synapses to quickly tune their output and maintain vesicle release during periods of high demand. The wide range in initial synaptic Munc18-1-Venus levels is in line with the notion that individual synapses can have very different release probabilities (Rosenmund et al., 1993; Murthy et al., 1997; Matz et al., 2010; Ariel et al., 2012). This presynaptic mechanism adds to other well-known factors that tune synaptic output like postsynaptic target identity (Reyes et al., 1998; Sylwestrak and Ghosh, 2012) and synaptic position on the dendrite (de Jong et al., 2012), and may partly underlie the effects of neuronal activity (Branco et al., 2008) and calcium influx (Ermolyuk et al., 2012) on synaptic output.

Reclustering of Munc18-1-Venus is PKC dependent and correlates with synaptic strength

Activation of the DAG–PKC pathway potentiates synaptic transmission (Malenka et al., 1986; Shapira et al., 1987) and is essential for post-tetanic potentiation (Brager et al., 2003; Fioravante et al., 2011). Furthermore, we have shown that DAG–PKC–dependent synaptic potentiation requires Munc18-1 phosphorylation, and that Munc18-1 phosphorylation is essential for maintaining synaptic release during repetitive stimulation and for synaptic recovery after stimulation (de Vries et al., 2000; Wierda et al., 2007). Here we show that Munc18-1-Venus reclustering after stimulation is calcium-dependent and almost absent after PKC inhibition. Moreover, a PKC-insensitive mutant Munc18-1 showed strongly impaired reclustering after intense stimulation. Thus, PKC-dependent phosphorylation of Munc18-1 is required for its reclustering and consequent changes in synaptic levels. Together, this provides a plausible mechanism for the fact that efficacy of synaptic vesicle release depends on Munc18-1 expression levels (Toonen et al., 2006b) and PKC activity (Majewski and Iannazzo, 1998; Stevens and Sullivan, 1998; Francis et al., 2002). We have previously shown that the PKC–Munc18-1 pathway translocates synaptic vesicles to the active zone (Wierda et al., 2007) and that Munc18-1 overexpression promotes membrane delivery of secretory vesicles in chromaffin cells (Toonen et al., 2006a). Hence, PKC-dependent recruitment of Munc18-1 temporarily increases its synaptic levels, thereby facilitating synaptic vesicle recruitment. Importantly, FM4-64 loading correlated with Munc18-1-Venus expression levels in individual synapses (Fig. 9). Moreover, synapses that recruited more Munc18-1 after high-frequency stimulation had a larger releasable vesicle pool. Hence, at the single synapse, Munc18-1 expression levels correlate with synaptic strength.

Together, our data support a model in which soluble Munc18-1 is dependent on plasma membrane–bound syntaxin-1 for delivery to the synapse at rest (Fig. 10, 1). At the synapse, Munc18-1 resides with syntaxin-1 and SNAP25 in microdomains at the plasma membrane (Lang et al., 2002; Sieber et al., 2006; Pertsinidis et al., 2013). Munc18-1 also interacts with other binding partners, and a fraction of Munc18-1 may transfer from syntaxin-1 (Fig. 10, 2) to these partners at some point after arrival in the synapse. Calcium influx temporarily increases Munc18-1 dynamics, which are independent of vesicle release or syntaxin-1 binding (Fig. 10, 3). Soluble Munc18-1 can disperse or may bind syntaxin-1 (Fig. 10, 4). After stimulation, PKC controls reclustering by phosphorylation of Munc18-1 (Fig. 10, 5). PKC-dependent reclustering of Munc18-1 temporarily increases the release of the synaptic vesicle pool.

Materials and methods

Generation of Munc18-1-Venus knockin mice

A Venus cDNA fragment from pVenus-N1 (Nagai et al., 2002) was subcloned using restriction enzymes (SmaI–NotI and SmaI, respectively) into pUC21 (Vieira and Messing, 1991), resulting in pUC21VENUS. A loxNEOlox cassette (containing neomycin resistance gene and thymidine kinase promoter flanked by two *LoxP* sites) was subcloned using SalI–XbaI into pUC21VENUS in an antisense orientation 3′ of the Venus stop codon. The left cloning arm, a genomic sequence 5′ of, and including, exon 20 of the *munc18-1* gene from 129/Sv embryonic stem (ES) cell DNA, was subcloned using PCR into pGEM-T Easy (Promega), resulting in pGEM-T Easy-Left-Arm. The right cloning arm, a genomic sequence 3′ of exon 20 of the *munc18-1* gene from 129/Sv ES cell DNA, was subcloned using PCR into pGEM-T Easy, resulting in pGEM-T Easy-Right-Arm. The right cloning arm was subcloned into pGEM-T Easy-Left-Arm using KpNI–AvrII and KpNI–SpeI.

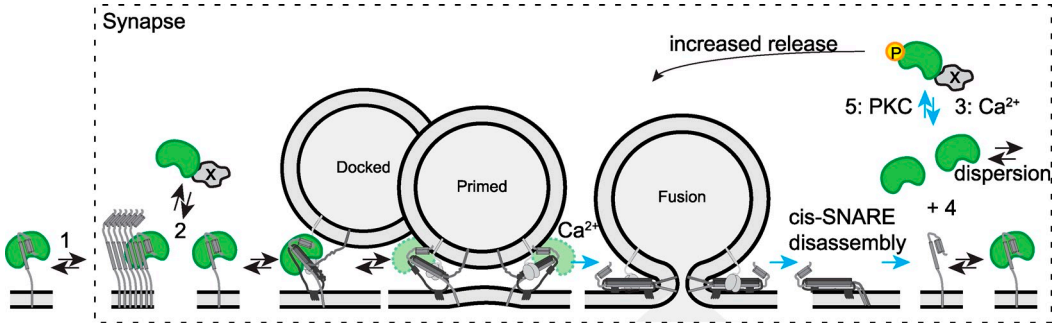

Figure 10. **Munc18-1 transport to and behavior in the synapse.** In mature neurons, Munc18-1 (shown in green) is transported to synapses via lateral diffusion with membrane-bound syntaxin-1 (shown in light gray, 1). At the synapse, Munc18-1 interacts with syntaxin-1 (individually or in microdomains) or dissociates and interacts with other binding partners (X; 2). Calcium influx triggers dissociation from binding partners (3) and temporarily increases free Munc18-1 concentrations in the synapse (4). After stimulation, PKC controls reclustering of Munc18-1 (5).

Venus and the loxNEOlox cassette from pUC21VENUS were subcloned between the left and right arm, with Venus replacing the stop codon of exon 20 in frame, creating the targeting vector (Fig. 1 A). Mice carrying the *munc18-1-venus-neo* gene were generated by homologous recombination in ES cells and identified by Southern blotting (Fig. 1 B) or PCR (Fig. 1 C). Heterozygous mice (+/m) were crossed with Ella-cre mice, which express Cre recombinase in early embryonic stages (Lakso et al., 1996), to remove the neomycin resistance cassette. All imaging experiments were conducted on hippocampal m/m neurons of +/m × +/m crosses. *Munc18-1* null mutant mice (deleting exon 2–6) have been described previously (Verhage et al., 2000). All animals were housed and bred according to the institutional and Dutch governmental guidelines for animal welfare.

Neuronal cultures and transfection

Dissociated hippocampal cultures were obtained from embryonic day 18 (E18) m/m mice as described previously (Meijer et al., 2012). In brief, hippocampi were dissected in Hepes-buffered HBBS (Invitrogen) and digested with 0.25% trypsin (Invitrogen) at 37°C for 20 min. After washing and trituration, cells were plated at a density of 25,000 cells/well for low-density cultures on top of a pregrown rat glia feeder layer on 18-mm coverslips. For autaptic cell cultures, cells were plated at a density of 2,000 cells/well on micro islands of rat glia as described previously (Meijer et al., 2012). Micro-islands were made by stamping 200-µm-diameter poly-D-lysine (0.15 mg/ml; Sigma-Aldrich)/rat tail collagen (3.66 mg/ml; BD) dots on 18-mm coverslips pretreated with 0.15% agarose (Type II-a). Cultures were kept in neurobasal medium (containing 2% B27, 18 mM Hepes, 0.5 mM GlutaMAX, and penicillin/streptomycin; all obtained from Invitrogen), and half the medium was replaced once every week in low-density cultures. Where applicable, Munc18-1-Venus neurons were cultured together with WT neurons in a 1:50 ratio to image single fluorescent neurons. Neurons were used for experiments at 14–21 DIV.

For imaging experiments on WT neurons, syntaxin-1-EYFP, GFP, mVenus, and synapsin-mCherry were transfected using calcium phosphate precipitate at 6–10 DIV as described previously (Köhrmann et al., 1999). For FM4-64 loading experiments in Munc18-1-Venus neurons, synapsin-ECFP was transfected using calcium phosphate precipitate at 6–10 DIV. For all other imaging experiments on Munc18-1-Venus neurons, synapsin-mCherry was expressed by adding lentiviral particles before plating. After trituration, lentiviral particles were added and cells were incubated at 37°C/5% CO_2 for 2 h. After three washes with neurobasal medium supplemented with 10% fetal bovine serum to inactivate the lentiviral particles, cells were plated on glia feeder layers. BoNT/C-ECFP was expressed using Semliki viral particles 6–12 h before imaging in autaptic cultures. ECFP signal in the soma of a single neuron on a micro island ensured BoNT/C expression in the imaged synapses.

For imaging of Munc18-1-EGFP and PKC-insensitive Munc18-1-EGFP on *munc18-1* null mutant neurons (Verhage et al., 2000), E18 embryos were obtained from timed *munc18-1* heterozygous null mutant matings and processed for WT neurons. Dissociated null mutant neurons were infected in solution before plating on glia micro islands with lentiviral particles expressing Munc18-1-EGFP WT or PKC-insensitive mutant together with synapsin-mCherry particles and placed in a cell culture incubator for 1.5 h. After two washing steps in MEM with 10% FCS, neurons were counted and plated at a density of 2,000 cells/18-mm coverslip.

Constructs

Syntaxin-1-EYFP is full-length rat Syntaxin1a in pEYFP-N1 (CMV promoter; Takara Bio Inc.), and has been described previously (Toonen et al., 2005). Expression plasmid pCMV BoNT/C light chain was a gift from T. Galli (Institut National de la Santé et de la Recherche Médicale, Paris, France). Synapsin-mCherry (pcDNA3.1) was a gift from A. Jeromin (Allen Brain Institute, Seattle, WA). Synapsin-ECFP was generated by replacing mCherry in Synapsin-mCherry with ECFP. mVenus was generated by the addition of the last 20 amino acids (KMSKDGKKKKKKSKTKCVIM) of K-Ras2B, representing a canonical palmitoylation signal (Welman et al., 2000). Synapsin-mCherry was subcloned into pLenti vectors, and viral particles were produced as described previously (Naldini et al., 1996). Munc18-1-EGFP WT and PKC-insensitive mutant Munc18-1-GFP ($Munc18_{PKCi}$: S306A, S312A, S313A; Wierda et al., 2007) were cloned into pLenti vectors and used to rescue *munc18-1* null mutant neurons.

Electrophysiological recordings

Electrophysiological recordings were performed on autaptic glutamatergic hippocampal neurons at room temperature (21–24°C) as described previously (Weber et al., 2010). In brief, isolated hippocampal neurons were plated on astrocyte micro islands (Bekkers and Stevens, 1991) in neurobasal medium (Invitrogen) supplemented with B-27 (Invitrogen), 17.3 mM Hepes, 1% GlutaMax-I (Invitrogen), and 1% penicillin/streptomycin (Invitrogen). Autaptic cells between 10 and 14 DIV were used for experiments. The patch-pipette solution included 135 mM potassium gluconate, 10 mM Hepes, 1 mM EGTA, 4.6 mM $MgCl_2$, 4 mM Na-ATP, 15 mM creatine phosphate, 50 U/ml phosphocreatine kinase, and 300 mOsm, pH 7.3. The standard extracellular medium consisted of 140 mM NaCl, 2.4 mM KCl, 10 mM Hepes, 10 mM glucose, 4 mM $CaCl_2$, 4 mM $MgCl_2$, and 300 mOsm, pH 7.3. Cells were whole-cell voltage clamped at −70 mV with an EPC-9 amplifier (HEKA) under control of Pulse 8.80 software (HEKA). Currents were low-pass filtered at 1 or 5 kHz and stored at either 10 or 20 kHz. Pipette resistance ranged from 4 to 6 MΩ. The series resistance was compensated for 75%. Only cells with series resistances <20 MΩ were analyzed. EPSCs were evoked by depolarizing the cell from −70 to 0 mV for 2 ms.

Immunochemistry

Cultured neurons from 1 to 14 DIV were fixed in 3.7% formaldehyde in PBS, pH 7.4, for 20 min at RT. Neurons were washed three times in PBS, permeabilized in 0.5% Triton X-100 (Sigma-Aldrich) in PBS for 5 min, and incubated with blocking solution (PBS containing 2% normal goat serum, 2% bovine serum albumin, and 0.1% Triton X-100) for 30 min at RT. Neurons were then incubated with primary antibodies in blocking solution for 1 h at RT, washed three times with PBS, and incubated with secondary antibodies conjugated to Alexa Fluor in blocking solution for 1 h at RT (1:1,000; Invitrogen). Primary antibodies used were chicken polyclonal MAP2 (1:20,000; Abcam), mouse monoclonal AnkyrinG (1:1,000; SC-12719; Santa Cruz Biotechnology, Inc.), Smi-312 (1:500; Covance), and polyclonal synapsin (1:2,000; Synaptic Systems). Finally, cells were washed three times in PBS and coverslips were mounted in Mowiol on glass slides. Images were acquired on a confocal microscope (LSM 510 Meta; Carl Zeiss) with a 63× oil objective lens, NA 1.4, and analyzed in MATLAB (MathWorks, Inc.) using SynD (Schmitz et al., 2011).

For labeling of brain slices, P14-P21 WT and Munc18-1-Venus mice were perfused transcardially with 4% PFA in PBS, then brains were removed and post-fixed in 4% PFA in PBS overnight. Subsequently, brains were submerged in 30% sucrose in PBS for 3 d before cryosectioning. Before incubation in blocking solution (5% normal goat serum, 2.5% BSA, and 0.2% Triton X-100 in PBS) for 1 h, 35-µm cryosections were incubated in 1% H_2O_2 for 30 min and rinsed with PBS. Sections were incubated with primary antibody in blocking solution overnight at 4°C on a shaker. Primary antibodies used were rabbit polyclonal Munc18-1b (1:200; Synaptic Systems), chicken polyclonal MAP2 (1:200; Abcam), and mouse monoclonal VAMP-2 (1:500; Synaptic Systems). Cryosections were then washed four times in PBS and incubated with secondary antibody (Alexa Fluor; Invitrogen) diluted in blocking solution for 2 h on a shaker. Finally, cryosections were mounted in 2.5% DABCO (Invitrogen) in Mowiol on glass slides. All steps were performed at RT, unless otherwise stated. Images were acquired on a confocal microscope (LSM 510 Meta; Carl Zeiss) with either a 10× air objective lens and 0.7× mechanical zoom (Fig. 1 G, top) or a 40× objective (1.3 NA) and 0.7× mechanical zoom (Fig. 1 G, bottom).

Live imaging

All live imaging experiments, except FM4-64 synapse labeling (Fig. 9), were conducted on a custom-built tandem illumination microscope (TIM; Olympus) consisting of an inverted imaging microscope (IX81; Olympus) and an upright laser scanning microscope. The inverted microscope part was used for imaging fluorescence using an MT20 light source (Olympus), appropriate filter sets (Semrock), and a 60× oil objective lens (NA 1.49) with or without a 1.6× additional magnification on an EM charge-coupled device (CCD) camera (C9100-02; Hamamatsu Photonics). Xcellence RT imaging software (Olympus) was used for controlling the microscope and recording the images.

FRAP. The upright microscope part (TIM; Olympus) guided and focused a 473-nm laser (full width at half maximum = ∼1 µm) used for fluorescence bleaching through a 60× water immersion objective lens (NA 0.90) on the plane of focus of the inverted microscope. For bleaching, one or multiple positions were selected and prepared in the Xcellence RT imaging software, and a transistor–transistor logic (TTL) pulse in between two imaging frames triggered the solid-state laser and laser scanner (UGA40; both from Rapp OptoElectronic). Laser intensity and pulse duration for bleaching were optimized to reach >60% fluorescence decrease. Fluorescence recovery was monitored by time-lapse acquisitions at 1–2 Hz for the first 30 s and 0.25–0.5 Hz for the remaining time.

FM4-64 synapse labeling. Experiments were conducted on an inverted microscope (Axio Observer Z; Carl Zeiss) for imaging fluorescence, using an illumination unit (Polychrome V; Till Photonics), appropriate filter sets (Chroma and Semrock), and a 40× oil objective lens (NA 1.30) equipped with automated focus adjustment (Definite Focus; Carl Zeiss) on an EM-CCD camera (C9100-02; Hamamatsu Photonics). Synaptic vesicle pools were labeled by field stimulation for 30 s at 1 Hz in the presence of 10 µM FM4-64 (Invitrogen). FM4-64, dissolved in imaging solution, was applied locally using a barrel pipette 30 s before, during, and 1 min after stimulation to ensure complete labeling of all recycling vesicles. The cells were subsequently washed by applying dye-free imaging solution for 15 min via the barrel pipette. The FM4-64 labeling experiments consisted of seven sequential steps: a baseline of 10 frames each (Synapsin-ECFP, Munc18-1-Venus, FM4-64); FM4-64 synapse labeling and wash with 1 frame each every 2 min; baseline of 10 frames each; 30 s of 600 AP at 20 Hz, or 600 AP at 2 Hz with 30 s of 0.2 Hz imaging + 5 min 1 frame every 30 s after Munc18-1-Venus reclustering; baseline of 10 frames each; FM4-64 synapse labeling and wash with 1 frame each every 2 min; baseline of 10 frames each; 30 s of 600 AP at 20 Hz; and baseline of 10 frames each.

Coverslips were placed in an imaging chamber and perfused with imaging solution (Tyrode's: 2 mM $CaCl_2$, 2.5 mM KCl, 119 mM NaCl, 2 mM $MgCl_2$, 20 mM glucose, and 25 mM Hepes, pH 7.4). Electrical field stimulation by parallel platinum electrodes was applied by a Master-8 system (A.M.P.I.), a stimulus isolator (A385RC; World Precision Instruments) delivering 30-mA, 1-ms pulses, and in the presence of 50 µM (2R)-amino-5-phosphonovaleric acid (AP5; Tocris Bioscience) and 10 µM 6,7-dinitroquinoxaline-2,3-dione (DNQX; Tocris Bioscience) to block network activity by inhibiting glutamatergic transmission. PMA (Sigma-Aldrich) was bath applied for long incubations (≥2 min) or barrel applied for short incubations (30 s). Ro 31-8220 (EMD Millipore) was bath applied. All imaging experiments were performed at RT (21–24°C).

Image analysis

Image stacks from time-lapse recordings were loaded into ImageJ (National Institutes of Health), and multiple regions of interest were placed: 6-pixel-diameter circles in the middle of bleached areas and/or unbleached synapses, background regions devoid of any cells, and a control region for acquisition bleaching. Raw traces were extracted and loaded into Excel (Microsoft) for further analysis. All raw traces were corrected for background with $F(t) = F_{raw}(t) - F_b(t)$, where $F_{raw}(t)$ and $F_b(t)$ are the intensity of a raw trace and the background trace, respectively, at time t, and subsequently corrected for ongoing photobleaching by multiplying with $F_{cntrl}(0)/F_{cntrl}(t)$, where $F_{cntrl}(0)$ is the background-corrected intensity of the control trace at time 0. For synaptic levels analysis, the corrected traces were normalized to the fluorescence at the start of the experiment with the following: $\Delta F/F0 = (F(t) - F(0))/F(0)$. For fluorescence recovery ($F_{rec}(t)$), the corrected traces of bleached regions were normalized to the fluorescence before ($F(t_{prebleach})$) and immediately after bleaching ($F(t_{bleach})$; Siggia et al., 2000) with:

$$F_{rec}(t) = \frac{F(t) - F(t_{bleach})}{F(t_{pre\text{-}bleach}) - F(t_{bleach})}.$$

A fit of the mean Munc18-1-Venus recovery trace was made according to a biexponential function:

$$F_{rec}(t) = M_f \times \left(1 - e^{\frac{-t}{\tau_f}}\right) + M_s \times \left(1 - e^{\frac{-t}{\tau_s}}\right),$$

where M_f and M_s are the mobile fraction of the fast and slow component, respectively, and τ_f and τ_s are the recovery time constants for the fast and slow component, respectively. The NonlinearLeastSquares function implemented in MATLAB was used to calculate the best fit. For synapse-to-axon ratio analysis, a linescan (width of 3 pixels) from the middle of the synapse (identified by Synapsin-mCherry) up to 4 µm into the axon (without passing other synapses) was extracted from an image loaded into ImageJ, and the trace was background corrected and normalized to intensity at the indicated lengths with $F_{norm}(x) = F(x)/F(x_a)$, where F(x) is the background-corrected fluorescence along the linescan and $F(x_a)$ is the background-corrected fluorescence at a specified point in the axon (x_a: 3–4 µm from synapse center). For kymographs, a line (width of 3 pixels) was placed over an axon in an image loaded into ImageJ, and the kymograph function was used accordingly.

Chemicals

Nimopedine, omega-agatoxin, and omega-conotoxin were obtained from Tocris Bioscience. Ro-31-8220 from Sigma-Aldrich. AP-V and DNQX were from Ascent.

Statistics

Differences between two groups were tested for significance using a Student's *t* test for unpaired data when data passed a normality test (Kolmogorov-Smirnov) and a Mann-Whitney (M-W) test when it did not. Differences between more than two groups were tested for significance using a Kruskal-Wallis (K-W) test, and pairwise comparisons using M-W tests were used where applicable. P-values were adjusted using a false discovery rate (FDR) correction (Benjamini and Hochberg, 1995) for the number of multiple comparisons in short FDR[number] corrections. For testing significant differences in the amount of synapses per group under different conditions, the Pearson's χ^2 test was used. Correlation between two variables was tested for significance with Spearman rank correlation. Differences were regarded as significant when $P < 0.05$. Statistics were performed in SPSS (IBM). All data are plotted as mean ± SEM (error bars or shaded area) in arbitrary units.

Online supplemental material

Fig. S1 shows protein expression levels in brain lysate of +/m and −/m mice together with example images of Munc18-1-Venus neuron morphology. Fig. S2 shows kymographs and quantification of bleached axons with and without transported vesicles. Fig. S3 shows the intensity change of mVenus during and after stimulation. Fig. S4 shows the relation between initial synaptic Munc18-1-Venus fluorescence and fluorescence after stimulation together with the relation between synaptic Munc18-1-Venus fluorescence and synapse size. Fig. S5 shows the intensity change of Munc18-1-Venus

subsets + P/Q-, L-, and N-type calcium channel blockers; Munc18-1-Venus FRAP + PMA; Munc18-1-Venus subsets + Ro 31-8220; and subsets of PKC-insensitive Munc18-1 mutant. Online supplemental material is available at http://www.jcb.org/cgi/content/full/jcb.201308026/DC1. Additional data are available in the JCB DataViewer at http://dx.doi.org/10.1083/jcb.201308026.dv.

We thank Robbert Zalm for expert help with virus production and cloning and Emmeke Aarts for excellent advice on statistics.

This work is supported by the Netherlands Organization for Scientific Research (ZonMw-VENI 916-66-101 and ZonMW-TOP 91208017 to R.F. Toonen, Pionier/VICI 900-01-001 and ZonMW 903-42-095 to M. Verhage, and ZonMw-TOP 91208017 to J.P. Weber). This work is also supported by the EU (EUSynapse project 019055, EUROSPIN project HEALTH-F2-2009-241498, and HEALTH-F2-2009-242167 SynSys project to M. Verhage).

The authors declare no competing financial interests.

T. Cijsouw, M. and R.F. Toonen designed the research; T. Cijsouw and J.H. Broeke performed and analyzed live cell imaging experiments; I. Saarloos, D. Schut, T. Kroon, and J.A.C. Broek performed biochemistry, and immunocytochemistry; J.P. Weber performed and analyzed electrophysiological recordings; and T. Cijsouw, M. Verhage, and R.F. Toonen wrote the manuscript.

Submitted: 5 August 2013
Accepted: 14 January 2014

References

Ariel, P., M.B. Hoppa, and T.A. Ryan. 2012. Intrinsic variability in Pv, RRP size, Ca^{2+} channel repertoire, and presynaptic potentiation in individual synaptic boutons. *Front Synaptic Neurosci*. 4:9.

Bekkers, J.M., and C.F. Stevens. 1991. Excitatory and inhibitory autaptic currents in isolated hippocampal neurons maintained in cell culture. *Proc. Natl. Acad. Sci. USA*. 88:7834–7838. http://dx.doi.org/10.1073/pnas.88.17.7834

Benjamini, Y., and Y. Hochberg. 1995. Controlling the False Discovery Rate: a Practical and Powerful Approach to Multiple Testing. *J. R. Stat. Soc. Series B Stat. Met*. 57:289–300.

Blasi, J., E.R. Chapman, S. Yamasaki, T. Binz, H. Niemann, and R. Jahn. 1993. Botulinum neurotoxin C1 blocks neurotransmitter release by means of cleaving HPC-1/syntaxin. *EMBO J.* 12:4821–4828.

Brager, D.H., X. Cai, and S.M. Thompson. 2003. Activity-dependent activation of presynaptic protein kinase C mediates post-tetanic potentiation. *Nat. Neurosci.* 6:551–552. http://dx.doi.org/10.1038/nn1067

Branco, T., K. Staras, K.J. Darcy, and Y. Goda. 2008. Local dendritic activity sets release probability at hippocampal synapses. *Neuron*. 59:475–485. http://dx.doi.org/10.1016/j.neuron.2008.07.006

Cai, Q., P.-Y. Pan, and Z.-H. Sheng. 2007. Syntabulin-kinesin-1 family member 5B-mediated axonal transport contributes to activity-dependent presynaptic assembly. *J. Neurosci.* 27:7284–7296. http://dx.doi.org/10.1523/JNEUROSCI.0731-07.2007

Chi, P., P. Greengard, and T.A. Ryan. 2001. Synapsin dispersion and reclustering during synaptic activity. *Nat. Neurosci.* 4:1187–1193. http://dx.doi.org/10.1038/nn756

Chua, J.J., E. Butkevich, J.M. Worseck, M. Kittelmann, M. Grønborg, E. Behrmann, U. Stelzl, N.J. Pavlos, M.M. Lalowski, S. Eimer, et al. 2012. Phosphorylation-regulated axonal dependent transport of syntaxin 1 is mediated by a Kinesin-1 adapter. *Proc. Natl. Acad. Sci. USA*. 109:5862–5867. http://dx.doi.org/10.1073/pnas.1113819109

Darcy, K.J., K. Staras, L.M. Collinson, and Y. Goda. 2006. Constitutive sharing of recycling synaptic vesicles between presynaptic boutons. *Nat. Neurosci.* 9:315–321. http://dx.doi.org/10.1038/nn1640

Davis, P.D., C.H. Hill, E. Keech, G. Lawton, J.S. Nixon, A.D. Sedgwick, J. Wadsworth, D. Westmacott, and S.E. Wilkinson. 1989. Potent selective inhibitors of protein kinase C. *FEBS Lett.* 259:61–63. http://dx.doi.org/10.1016/0014-5793(89)81494-2

de Jong, A.P., S.K. Schmitz, R.F. Toonen, and M. Verhage. 2012. Dendritic position is a major determinant of presynaptic strength. *J. Cell Biol.* 197:327–337. http://dx.doi.org/10.1083/jcb.201112135

de Vries, K.J., A. Geijtenbeek, E.C. Brian, P.N. de Graan, W.E. Ghijsen, and M. Verhage. 2000. Dynamics of munc18-1 phosphorylation/dephosphorylation in rat brain nerve terminals. *Eur. J. Neurosci.* 12:385–390. http://dx.doi.org/10.1046/j.1460-9568.2000.00931.x

de Wit, H., L.N. Cornelisse, R.F.G. Toonen, and M. Verhage. 2006. Docking of secretory vesicles is syntaxin dependent. *PLoS ONE*. 1:e126. http://dx.doi.org/10.1371/journal.pone.0000126

Degtyar, V., I.M. Hafez, C. Bray, and R.S. Zucker. 2013. Dance of the SNAREs: assembly and rearrangements detected with FRET at neuronal synapses. *J. Neurosci.* 33:5507–5523. http://dx.doi.org/10.1523/JNEUROSCI.2337-12.2013

Denker, A., K. Kröhnert, J. Bückers, E. Neher, and S.O. Rizzoli. 2011. The reserve pool of synaptic vesicles acts as a buffer for proteins involved in synaptic vesicle recycling. *Proc. Natl. Acad. Sci. USA*. 108:17183–17188. http://dx.doi.org/10.1073/pnas.1112690108

Dulubova, I., S. Sugita, S. Hill, M. Hosaka, I. Fernandez, T.C. Südhof, and J. Rizo. 1999. A conformational switch in syntaxin during exocytosis: role of munc18. *EMBO J.* 18:4372–4382. http://dx.doi.org/10.1093/emboj/18.16.4372

Ermolyuk, Y.S., F.G. Alder, C. Henneberger, D.A. Rusakov, D.M. Kullmann, and K.E. Volynski. 2012. Independent regulation of basal neurotransmitter release efficacy by variable Ca^{2+} influx and bouton size at small central synapses. *PLoS Biol.* 10:e1001396. http://dx.doi.org/10.1371/journal.pbio.1001396

Fernández-Alfonso, T., R. Kwan, and T.A. Ryan. 2006. Synaptic vesicles interchange their membrane proteins with a large surface reservoir during recycling. *Neuron*. 51:179–186. http://dx.doi.org/10.1016/j.neuron.2006.06.008

Fioravante, D., Y. Chu, M.H. Myoga, M. Leitges, and W.G. Regehr. 2011. Calcium-dependent isoforms of protein kinase C mediate posttetanic potentiation at the calyx of Held. *Neuron*. 70:1005–1019. http://dx.doi.org/10.1016/j.neuron.2011.04.019

Francis, H.W., J.C. Scott, and P.B. Manis. 2002. Protein kinase C mediates potentiation of synaptic transmission by phorbol ester at parallel fibers in the dorsal cochlear nucleus. *Brain Res.* 951:9–22. http://dx.doi.org/10.1016/S0006-8993(02)03095-0

Garcia, E.P., E. Gatti, M. Butler, J. Burton, and P. De Camilli. 1994. A rat brain Sec1 homologue related to Rop and UNC18 interacts with syntaxin. *Proc. Natl. Acad. Sci. USA*. 91:2003–2007. http://dx.doi.org/10.1073/pnas.91.6.2003

Garcia, E.P., P.S. McPherson, T.J. Chilcote, K. Takei, and P. De Camilli. 1995. rbSec1A and B colocalize with syntaxin 1 and SNAP-25 throughout the axon, but are not in a stable complex with syntaxin. *J. Cell Biol.* 129:105–120. http://dx.doi.org/10.1083/jcb.129.1.105

Hamdan, F.F., A. Piton, J. Gauthier, A. Lortie, F. Dubeau, S. Dobrzeniecka, D. Spiegelman, A. Noreau, S. Pellerin, M. Côté, et al. 2009. De novo STXBP1 mutations in mental retardation and nonsyndromic epilepsy. *Ann. Neurol.* 65:748–753. http://dx.doi.org/10.1002/ana.21625

Hata, Y., C.A. Slaughter, and T.C. Südhof. 1993. Synaptic vesicle fusion complex contains unc-18 homologue bound to syntaxin. *Nature*. 366:347–351. http://dx.doi.org/10.1038/366347a0

Herzog, E., F. Nadrigny, K. Silm, C. Biesemann, I. Helling, T. Bersot, H. Steffens, R. Schwartzmann, U.V. Nägerl, S. El Mestikawy, et al. 2011. In vivo imaging of intersynaptic vesicle exchange using VGLUT1 Venus knock-in mice. *J. Neurosci.* 31:15544–15559. http://dx.doi.org/10.1523/JNEUROSCI.2073-11.2011

Jacobs, E.H., R.J. Williams, and P.T. Francis. 2006. Cyclin-dependent kinase 5, Munc18a and Munc18-interacting protein 1/X11α protein up-regulation in Alzheimer's disease. *Neuroscience*. 138:511–522. http://dx.doi.org/10.1016/j.neuroscience.2005.11.017

Jahn, R., and D. Fasshauer. 2012. Molecular machines governing exocytosis of synaptic vesicles. *Nature*. 490:201–207. http://dx.doi.org/10.1038/nature11320

Jahn, R., and R.H. Scheller. 2006. SNAREs—engines for membrane fusion. *Nat. Rev. Mol. Cell Biol.* 7:631–643. http://dx.doi.org/10.1038/nrm2002

Kalla, S., M. Stern, J. Basu, F. Varoqueaux, K. Reim, C. Rosenmund, N.E. Ziv, and N. Brose. 2006. Molecular dynamics of a presynaptic active zone protein studied in Munc13-1-enhanced yellow fluorescent protein knock-in mutant mice. *J. Neurosci.* 26:13054–13066. http://dx.doi.org/10.1523/JNEUROSCI.4330-06.2006

Köhrmann, M., M. Luo, C. Kaether, L. DesGroseillers, C.G. Dotti, and M.A. Kiebler. 1999. Microtubule-dependent recruitment of Staufen-green fluorescent protein into large RNA-containing granules and subsequent dendritic transport in living hippocampal neurons. *Mol. Biol. Cell*. 10:2945–2953. http://dx.doi.org/10.1091/mbc.10.9.2945

Lakso, M., J.G. Pichel, J.R. Gorman, B. Sauer, Y. Okamoto, E. Lee, F.W. Alt, and H. Westphal. 1996. Efficient in vivo manipulation of mouse genomic sequences at the zygote stage. *Proc. Natl. Acad. Sci. USA*. 93:5860–5865. http://dx.doi.org/10.1073/pnas.93.12.5860

Lang, T., M. Margittai, H. Hölzler, and R. Jahn. 2002. SNAREs in native plasma membranes are active and readily form core complexes with endogenous and exogenous SNAREs. *J. Cell Biol.* 158:751–760. http://dx.doi.org/10.1083/jcb.200203088

Li, Z., and V.N. Murthy. 2001. Visualizing postendocytic traffic of synaptic vesicles at hippocampal synapses. *Neuron*. 31:593–605. http://dx.doi.org/10.1016/S0896-6273(01)00398-1

Majewski, H., and L. Iannazzo. 1998. Protein kinase C: a physiological mediator of enhanced transmitter output. *Prog. Neurobiol.* 55:463–475. http://dx.doi.org/10.1016/S0301-0082(98)00017-3

Malenka, R.C., D.V. Madison, and R.A. Nicoll. 1986. Potentiation of synaptic transmission in the hippocampus by phorbol esters. *Nature*. 321:175–177. http://dx.doi.org/10.1038/321175a0

Mastrangelo, M., A. Peron, L. Spaccini, F. Novara, B. Scelsa, P. Introvini, F. Raviglione, S. Faiola, and O. Zuffardi. 2013. Neonatal suppression-burst without epileptic seizures: expanding the electroclinical phenotype of STXBP1-related, early-onset encephalopathy. *Epileptic Disord.* 15:55–61.

Matz, J., A. Gilyan, A. Kolar, T. McCarvill, and S.R. Krueger. 2010. Rapid structural alterations of the active zone lead to sustained changes in neurotransmitter release. *Proc. Natl. Acad. Sci. USA*. 107:8836–8841. http://dx.doi.org/10.1073/pnas.0906087107

McEwen, J.M., and J.M. Kaplan. 2008. UNC-18 promotes both the anterograde trafficking and synaptic function of syntaxin. *Mol. Biol. Cell*. 19:3836–3846. http://dx.doi.org/10.1091/mbc.E08-02-0160

Medine, C.N., C. Rickman, L.H. Chamberlain, and R.R. Duncan. 2007. Munc18-1 prevents the formation of ectopic SNARE complexes in living cells. *J. Cell Sci.* 120:4407–4415. http://dx.doi.org/10.1242/jcs.020230

Meijer, M., P. Burkhardt, H. de Wit, R.F. Toonen, D. Fasshauer, and M. Verhage. 2012. Munc18-1 mutations that strongly impair SNARE-complex binding support normal synaptic transmission. *EMBO J.* 31:2156–2168. http://dx.doi.org/10.1038/emboj.2012.72

Milh, M., N. Villeneuve, M. Chouchane, A. Kaminska, C. Laroche, M.A. Barthez, C. Gitiaux, C. Bartoli, A. Borges-Correia, P. Cacciagli, et al. 2011. Epileptic and nonepileptic features in patients with early onset epileptic encephalopathy and STXBP1 mutations. *Epilepsia*. 52:1828–1834. http://dx.doi.org/10.1111/j.1528-1167.2011.03181.x

Misura, K.M., R.H. Scheller, and W.I. Weis. 2000. Three-dimensional structure of the neuronal-Sec1-syntaxin 1a complex. *Nature*. 404:355–362. http://dx.doi.org/10.1038/35006120

Mitchell, S.J., and T.A. Ryan. 2004. Syntaxin-1A is excluded from recycling synaptic vesicles at nerve terminals. *J. Neurosci.* 24:4884–4888. http://dx.doi.org/10.1523/JNEUROSCI.0174-04.2004

Murthy, V.N., T.J. Sejnowski, and C.F. Stevens. 1997. Heterogeneous release properties of visualized individual hippocampal synapses. *Neuron*. 18:599–612. http://dx.doi.org/10.1016/S0896-6273(00)80301-3

Nagai, T., K. Ibata, E.S. Park, M. Kubota, K. Mikoshiba, and A. Miyawaki. 2002. A variant of yellow fluorescent protein with fast and efficient maturation for cell-biological applications. *Nat. Biotechnol.* 20:87–90. http://dx.doi.org/10.1038/nbt0102-87

Naldini, L., U. Blömer, P. Gallay, D. Ory, R. Mulligan, F.H. Gage, I.M. Verma, and D. Trono. 1996. In vivo gene delivery and stable transduction of nondividing cells by a lentiviral vector. *Science*. 272:263–267. http://dx.doi.org/10.1126/science.272.5259.263

Nili, U., H. de Wit, A. Gulyas-Kovacs, R.F. Toonen, J.B. Sørensen, M. Verhage, and U. Ashery. 2006. Munc18-1 phosphorylation by protein kinase C potentiates vesicle pool replenishment in bovine chromaffin cells. *Neuroscience*. 143:487–500. http://dx.doi.org/10.1016/j.neuroscience.2006.08.014

Orenbuch, A., Y. Shulman, N. Lipstein, A. Bechar, Y. Lavy, E. Brumer, M. Vasileva, J. Kahn, L. Barki-Harrington, T. Kuner, and D. Gitler. 2012a. Inhibition of exocytosis or endocytosis blocks activity-dependent redistribution of synapsin. *J. Neurochem.* 120:248–258. (published erratum appears in *J. Neurochem*. 2012. 121:180) http://dx.doi.org/10.1111/j.1471-4159.2011.07579.x

Orenbuch, A., L. Shalev, V. Marra, I. Sinai, Y. Lavy, J. Kahn, J.J. Burden, K. Staras, and D. Gitler. 2012b. Synapsin selectively controls the mobility of resting pool vesicles at hippocampal terminals. *J. Neurosci.* 32:3969–3980. http://dx.doi.org/10.1523/JNEUROSCI.5058-11.2012

Pertsinidis, A., K. Mukherjee, M. Sharma, Z.P. Pang, S.R. Park, Y. Zhang, A.T. Brunger, T.C. Südhof, and S. Chu. 2013. Ultrahigh-resolution imaging reveals formation of neuronal SNARE/Munc18 complexes in situ. *Proc. Natl. Acad. Sci. USA*. 110:E2812–E2820. http://dx.doi.org/10.1073/pnas.1310654110

Pevsner, J., S.C. Hsu, and R.H. Scheller. 1994. n-Sec1: a neural-specific syntaxin-binding protein. *Proc. Natl. Acad. Sci. USA*. 91:1445–1449. http://dx.doi.org/10.1073/pnas.91.4.1445

Reyes, A., R. Lujan, A. Rozov, N. Burnashev, P. Somogyi, and B. Sakmann. 1998. Target-cell-specific facilitation and depression in neocortical circuits. *Nat. Neurosci.* 1:279–285. http://dx.doi.org/10.1038/1092

Ribrault, C., J. Reingruber, M. Petković, T. Galli, N.E. Ziv, D. Holcman, and A. Triller. 2011. Syntaxin1A lateral diffusion reveals transient and local SNARE interactions. *J. Neurosci.* 31:17590–17602. http://dx.doi.org/10.1523/JNEUROSCI.4065-11.2011

Rizo, J., and T.C. Südhof. 2012. The membrane fusion enigma: SNAREs, Sec1/Munc18 proteins, and their accomplices—guilty as charged? *Annu. Rev. Cell Dev. Biol.* 28:279–308. http://dx.doi.org/10.1146/annurev-cellbio-101011-155818

Rosenmund, C., J.D. Clements, and G.L. Westbrook. 1993. Nonuniform probability of glutamate release at a hippocampal synapse. *Science*. 262:754–757. http://dx.doi.org/10.1126/science.7901909

Rowe, J., F. Calegari, E. Taverna, R. Longhi, and P. Rosa. 2001. Syntaxin 1A is delivered to the apical and basolateral domains of epithelial cells: the role of munc-18 proteins. *J. Cell Sci.* 114:3323–3332.

Saitsu, H., M. Kato, T. Mizuguchi, K. Hamada, H. Osaka, J. Tohyama, K. Uruno, S. Kumada, K. Nishiyama, A. Nishimura, et al. 2008. De novo mutations in the gene encoding STXBP1 (MUNC18-1) cause early infantile epileptic encephalopathy. *Nat. Genet.* 40:782–788. http://dx.doi.org/10.1038/ng.150

Sankaranarayanan, S., P.P. Atluri, and T.A. Ryan. 2003. Actin has a molecular scaffolding, not propulsive, role in presynaptic function. *Nat. Neurosci.* 6:127–135. http://dx.doi.org/10.1038/nn1002

Schiavo, G., C.C. Shone, M.K. Bennett, R.H. Scheller, and C. Montecucco. 1995. Botulinum neurotoxin type C cleaves a single Lys-Ala bond within the carboxyl-terminal region of syntaxins. *J. Biol. Chem.* 270:10566–10570. http://dx.doi.org/10.1074/jbc.270.18.10566

Schmitz, S.K., J.J. Hjorth, R.M. Joemai, R. Wijntjes, S. Eijgenraam, P. de Bruijn, C. Georgiou, A.P. de Jong, A. van Ooyen, M. Verhage, et al. 2011. Automated analysis of neuronal morphology, synapse number and synaptic recruitment. *J. Neurosci. Methods*. 195:185–193. (published erratum appears in *J. Neurosci. Methods*. 2011. 197:190) http://dx.doi.org/10.1016/j.jneumeth.2010.12.011

Schröder, M.S., A. Stellmacher, S. Romorini, C. Marini, C. Montenegro-Venegas, W.D. Altrock, E.D. Gundelfinger, and A. Fejtova. 2013. Regulation of presynaptic anchoring of the scaffold protein Bassoon by phosphorylation-dependent interaction with 14-3-3 adaptor proteins. *PLoS ONE*. 8:e58814. http://dx.doi.org/10.1371/journal.pone.0058814

Shapira, R., S.D. Silberberg, S. Ginsburg, and R. Rahamimoff. 1987. Activation of protein kinase C augments evoked transmitter release. *Nature*. 325:58–60. http://dx.doi.org/10.1038/325058a0

Sieber, J.J., K.I. Willig, R. Heintzmann, S.W. Hell, and T. Lang. 2006. The SNARE motif is essential for the formation of syntaxin clusters in the plasma membrane. *Biophys. J.* 90:2843–2851. http://dx.doi.org/10.1529/biophysj.105.079574

Siggia, E.D., J. Lippincott-Schwartz, and S. Bekiranov. 2000. Diffusion in inhomogeneous media: theory and simulations applied to whole cell photobleach recovery. *Biophys. J.* 79:1761–1770. http://dx.doi.org/10.1016/S0006-3495(00)76428-9

Spangler, S.A., S.K. Schmitz, J.T. Kevenaar, E. de Graaff, H. de Wit, J. Demmers, R.F. Toonen, and C.C. Hoogenraad. 2013. Liprin-α2 promotes the presynaptic recruitment and turnover of RIM1/CASK to facilitate synaptic transmission. *J. Cell Biol.* 201:915–928. http://dx.doi.org/10.1083/jcb.201301011

Star, E.N., A.J. Newton, and V.N. Murthy. 2005. Real-time imaging of Rab3a and Rab5a reveals differential roles in presynaptic function. *J. Physiol.* 569:103–117. http://dx.doi.org/10.1113/jphysiol.2005.092528

Staras, K., T. Branco, J.J. Burden, K. Pozo, K. Darcy, V. Marra, A. Ratnayaka, and Y. Goda. 2010. A vesicle superpool spans multiple presynaptic terminals in hippocampal neurons. *Neuron*. 66:37–44. http://dx.doi.org/10.1016/j.neuron.2010.03.020

Stevens, C.F., and J.M. Sullivan. 1998. Regulation of the readily releasable vesicle pool by protein kinase C. *Neuron*. 21:885–893. http://dx.doi.org/10.1016/S0896-6273(00)80603-0

Su, Q., Q. Cai, C. Gerwin, C.L. Smith, and Z.-H. Sheng. 2004. Syntabulin is a microtubule-associated protein implicated in syntaxin transport in neurons. *Nat. Cell Biol.* 6:941–953. http://dx.doi.org/10.1038/ncb1169

Sylwestrak, E.L., and A. Ghosh. 2012. Elfn1 regulates target-specific release probability at CA1-interneuron synapses. *Science*. 338:536–540. http://dx.doi.org/10.1126/science.1222482

Toonen, R.F., and M. Verhage. 2007. Munc18-1 in secretion: lonely Munc joins SNARE team and takes control. *Trends Neurosci.* 30:564–572. http://dx.doi.org/10.1016/j.tins.2007.08.008

Toonen, R.F., K.J. de Vries, R. Zalm, T.C. Südhof, and M. Verhage. 2005. Munc18-1 stabilizes syntaxin 1, but is not essential for syntaxin 1 targeting and SNARE complex formation. *J. Neurochem.* 93:1393–1400. http://dx.doi.org/10.1111/j.1471-4159.2005.03128.x

Toonen, R.F., O. Kochubey, H. de Wit, A. Gulyas-Kovacs, B. Konijnenburg, J.B. Sørensen, J. Klingauf, and M. Verhage. 2006a. Dissecting docking and tethering of secretory vesicles at the target membrane. *EMBO J.* 25:3725–3737. http://dx.doi.org/10.1038/sj.emboj.7601256

Toonen, R.F., K. Wierda, M.S. Sons, H. de Wit, L.N. Cornelisse, A. Brussaard, J.J. Plomp, and M. Verhage. 2006b. Munc18-1 expression levels control synapse recovery by regulating readily releasable pool size. *Proc.*

Natl. Acad. Sci. USA. 103:18332–18337. http://dx.doi.org/10.1073/pnas.0608507103

Tsuriel, S., R. Geva, P. Zamorano, T. Dresbach, T. Boeckers, E.D. Gundelfinger, C.C. Garner, and N.E. Ziv. 2006. Local sharing as a predominant determinant of synaptic matrix molecular dynamics. *PLoS Biol.* 4:e271. http://dx.doi.org/10.1371/journal.pbio.0040271

Tsuriel, S., A. Fisher, N. Wittenmayer, T. Dresbach, C.C. Garner, and N.E. Ziv. 2009. Exchange and redistribution dynamics of the cytoskeleton of the active zone molecule bassoon. *J. Neurosci.* 29:351–358. http://dx.doi.org/10.1523/JNEUROSCI.4777-08.2009

Urigüen, L., I. Gil-Pisa, E. Munarriz-Cuezva, E. Berrocoso, J. Pascau, M.L. Soto-Montenegro, A. Gutiérrez-Adán, B. Pintado, J.L. Madrigal, E. Castro, et al. 2013. Behavioral, neurochemical and morphological changes induced by the overexpression of munc18-1a in brain of mice: relevance to schizophrenia. *Transl. Psychiatry*. 3:e221. http://dx.doi.org/10.1038/tp.2012.149

Vatta, M., M.B. Tennison, A.S. Aylsworth, C.M. Turcott, M.P. Guerra, C.M. Eng, and Y. Yang. 2012. A novel STXBP1 mutation causes focal seizures with neonatal onset. *J. Child Neurol.* 27:811–814. http://dx.doi.org/10.1177/0883073811435246

Verhage, M., A.S. Maia, J.J. Plomp, A.B. Brussaard, J.H. Heeroma, H. Vermeer, R.F. Toonen, R.E. Hammer, T.K. van den Berg, M. Missler, et al. 2000. Synaptic assembly of the brain in the absence of neurotransmitter secretion. *Science*. 287:864–869. http://dx.doi.org/10.1126/science.287.5454.864

Vieira, J., and J. Messing. 1991. New pUC-derived cloning vectors with different selectable markers and DNA replication origins. *Gene*. 100:189–194. http://dx.doi.org/10.1016/0378-1119(91)90365-I

Voets, T., R.F. Toonen, E.C. Brian, H. de Wit, T. Moser, J. Rettig, T.C. Südhof, E. Neher, and M. Verhage. 2001. Munc18-1 promotes large dense-core vesicle docking. *Neuron*. 31:581–592. http://dx.doi.org/10.1016/S0896-6273(01)00391-9

Weber, J.P., K. Reim, and J.B. Sørensen. 2010. Opposing functions of two sub-domains of the SNARE-complex in neurotransmission. *EMBO J.* 29:2477–2490. http://dx.doi.org/10.1038/emboj.2010.130

Welman, A., M.M. Burger, and J. Hagmann. 2000. Structure and function of the C-terminal hypervariable region of K-Ras4B in plasma membrane targetting and transformation. *Oncogene*. 19:4582–4591. http://dx.doi.org/10.1038/sj.onc.1203818

Wierda, K.D., R.F. Toonen, H. de Wit, A.B. Brussaard, and M. Verhage. 2007. Interdependence of PKC-dependent and PKC-independent pathways for presynaptic plasticity. *Neuron*. 54:275–290. http://dx.doi.org/10.1016/j.neuron.2007.04.001

Xu, Y., L. Su, and J. Rizo. 2010. Binding of Munc18-1 to synaptobrevin and to the SNARE four-helix bundle. *Biochemistry*. 49:1568–1576. http://dx.doi.org/10.1021/bi9021878

Zhou, P., Z.P. Pang, X. Yang, Y. Zhang, C. Rosenmund, T. Bacaj, and T.C. Südhof. 2013. Syntaxin-1 N-peptide and Habc-domain perform distinct essential functions in synaptic vesicle fusion. *EMBO J.* 32:159–171. http://dx.doi.org/10.1038/emboj.2012.307